

Intricate Hollow Structures: Controlled Synthesis and Applications in Energy Storage and Conversion

Liang Zhou,* Zechao Zhuang, Huihui Zhao, Mengting Lin, Dongyuan Zhao, and Liqiang Mai*

Intricate hollow structures garner tremendous interest due to their aesthetic beauty, unique structural features, fascinating physicochemical properties, and widespread applications. Here, the recent advances in the controlled synthesis are discussed, as well as applications of intricate hollow structures with regard to energy storage and conversion. The synthetic strategies toward complex multishelled hollow structures are classified into six categories, including well-established hard- and soft-templating methods, as well as newly emerging approaches based on selective etching of “soft@hard” particles, Ostwald ripening, ion exchange, and thermally induced mass relocation. Strategies for constructing structures beyond multishelled hollow structures, such as bubble-within-bubble, tube-in-tube, and wire-in-tube structures, are also covered. Niche applications of intricate hollow structures in lithium-ion batteries, Li–S batteries, supercapacitors, Li–O₂ batteries, dye-sensitized solar cells, photocatalysis, and fuel cells are discussed in detail. Some perspectives on the future research and development of intricate hollow structures are also provided.

and multiple interior cavities. Recently, intricate hollow structures have attracted tremendous attention in research.^[1,3,9,16] Such attention is not only from the point of view of purely fundamental interest as materials scientists always strive to create materials with the highest degree of complexity and aesthetic beauty, but also from application demands, since the functional materials used in practical applications are getting increasingly complex.^[1] Compared with simple hollow structures, their intricate counterparts are expected to offer more opportunities to tailor their physicochemical properties by manipulating the structure at micro-/nanoscale. The tailored physicochemical properties in turn enable intricate hollow structures with optimized performance in certain applications, outperforming simple hollow structures and bulk materials.

1. Introduction

Hollow structures refer to materials with well-defined boundaries and interior cavities.^[1] As a unique family of functional materials, they possess low density and high pore volume, as well as reduced mass- and charge-transport lengths. These unique structural features endow hollow structures with broad applications in nanoreactors, gas sensors, drug delivery, water treatment, secondary batteries, supercapacitors, dye-sensitized solar cells (DSSCs), photocatalysis, fuel cells, etc.^[2–19]

Based on their structural complexity, hollow structures can be classified into simple ones and intricate ones. Simple hollow structures, also known-as single-shelled hollow structures, have a single shell encapsulating a cavity at the center. Intricate hollow structures, on the other hand, have multiple boundaries

In the specific field of energy storage and conversion, intricate hollow structures are playing a more and more important role. More importantly, they hold great promise to break some of the current bottlenecks in secondary batteries, supercapacitors, fuel cells, DSSCs, photocatalysis, and fuel cells.^[9] For example, the cavity of intricate hollow structures can effectively accommodate the volume change of high-capacity lithium-ion battery (LIB) anode materials, such as transition-metal oxides (TMOs), Sn, and Si, boosting the cycling stability. In lithium–sulfur (Li–S) batteries, such unique structures are able to reserve a large amount of sulfur (S), accommodate the volume variation of S during cycling, and avoid the discharged products from dissolution through either physical confinement or chemical interactions. If nanopores are created on the shell, intricate hollow structures can provide a high specific surface area for charge storage in supercapacitors, as well as more-accessible active sites for lithium–air (Li–O₂) batteries and fuel cells. In DSSCs and photocatalysis, intricate hollow structures have the unique advantages of enabling multiple light reflection and scattering, leading to enhanced light-harvesting capability and thus superior power conversion efficiency or photocatalytic activity.

A number of high-quality reviews have been published in the last decade covering the synthesis and applications of hollow structures without specific focus on intricate hollow structures.^[2,4–8,10–15,17–21] Recently, several reviews have discussed some aspects of complex hollow structures and their applications in energy storage and conversion, gas sensors,

Prof. L. Zhou, Z. C. Zhuang, H. H. Zhao, M. T. Lin,
Prof. D. Y. Zhao, Prof. L. Q. Mai
State Key Laboratory of Advanced Technology
for Materials Synthesis and Processing
International School of
Materials Science and Engineering
Wuhan University of Technology
Wuhan 430070, Hubei, P. R. China
E-mail: liangzhou@whut.edu.cn; mlq518@whut.edu.cn



DOI: 10.1002/adma.201602914

and biomedicine.^[1,3,9,16] Here, we make great efforts to present a comprehensive overview of the synthetic methodologies for intricate hollow structures with special emphasis on newly emerging synthetic strategies. The application of intricate hollow structures in LIBs, Li-S batteries, supercapacitors, Li-O₂ batteries, DSSCs, photocatalysis, and fuel cells is also highlighted.

2. Synthetic Methodologies for Multi-Shelled Hollow Structures

Multishelled hollow structures (MSHSs), also known as Matryoshkas or Russian dolls, are the most frequently studied intricate hollow structures. They have multiple concentric or eccentric shells with different sizes. Because of their complex structure, the synthesis and manipulation of intricate hollow structures are much more challenging than those of their single-shelled counterparts. It is generally accepted that the more complicated a target structure is, the more sophisticated a synthetic procedure is needed.^[22] As a result, some special synthetic strategies different from routine methods toward single-shelled hollow structures, are required to achieve intricate hollow structures. In this section, the synthetic methodologies for MSHSs, including well-established hard- and soft-templating methods, as well as newly emerging approaches based on selective etching of “soft@hard” particles, Ostwald ripening, ion exchange and thermally induced mass relocation, will be comprehensively reviewed.

2.1. Hard Templating

Hard templating is the most widely employed method for the production of hollow structures; it is simple, effective, and straightforward in concept. Early in 1998, Caruso et al. pioneered the synthesis of hollow spheres by combining colloidal templating and shell-by-shell deposition.^[23] In general, the hard-templating synthesis involves four major steps: i) template preparation; ii) surface modification of the hard template, iii) target material coating/deposition; and iv) template removal.^[2] The coating/deposition of the target material on a hard template (step II) is generally considered as the most challenging step; sometimes, the surface modification (step III) can be omitted if the target material is compatible with the template. The most frequently employed hard templates include monodisperse polymer, silica, carbon, metal, and metal oxide colloids. These templates are selected because of their monodispersity, easy size and shape control, ready availability in large amounts, and easy synthesis using well-known recipes. For example, monodisperse silica (SiO₂) spheres with controllable size can be easily prepared by the Stöber process on a large scale.^[24]

2.1.1. Templating against Solid Hard Templates

Conceptually, it is feasible to extend the hard-templating method to the fabrication of MSHSs. For the preparation of MSHSs, the target shells and sacrificial interlayers are



Liang Zhou received his B.S. (2006) and Ph.D. (2011) from Fudan University (with Prof. Dongyuan Zhao and Prof. Chengzhong Yu). He then carried out postdoctoral research in Prof. Xiong Wen (David) Lou's group at Nanyang Technological University and Prof. Chengzhong Yu's

group at The University of Queensland. He is currently a Professor at Wuhan University of Technology. His research interests focus on functional nanomaterials for energy storage and conversion applications.



Dongyuan Zhao received his B.S. (1984) and Ph.D. (1990) from Jilin University. He is currently a Professor at Fudan University and has a high-level consulting Professorship at Wuhan University of Technology. He was selected as an academician of the Chinese Academy of Science in 2007, and a member of The Word Academy of

Science in 2010. His research interests focus on the synthesis of ordered mesoporous materials for catalysis, energy, water purification, and biomedicine applications.



Liqiang Mai received his Ph.D. degree from Wuhan University of Technology in 2004. He then carried out postdoctoral research in Prof. Zhonglin Wang's group at Georgia Institute of Technology (2006–2007) and worked as an advanced research scholar in Prof. Charles M. Lieber's group at Harvard University

(2008–2011). He is currently a Chair Professor at Wuhan University of Technology. His research interests include nanowires, micro-/nano-energy-storage devices, and energy-based nano-bio interfaces.

sequentially coated onto the template; after removing the sacrificial template and interlayers, MSHSs can be obtained.^[16] For example, Jang and co-workers reported the hard-templating synthesis of TiO₂ hollow spheres with controllable shell numbers (**Figure 1a**).^[25] In this approach, SiO₂ spheres prepared by the Stöber process are employed as the hard templates. TiO₂ and SiO₂ layers are alternately coated on the surface of SiO₂ spheres to form SiO₂@TiO₂, SiO₂@TiO₂@SiO₂@TiO₂, and

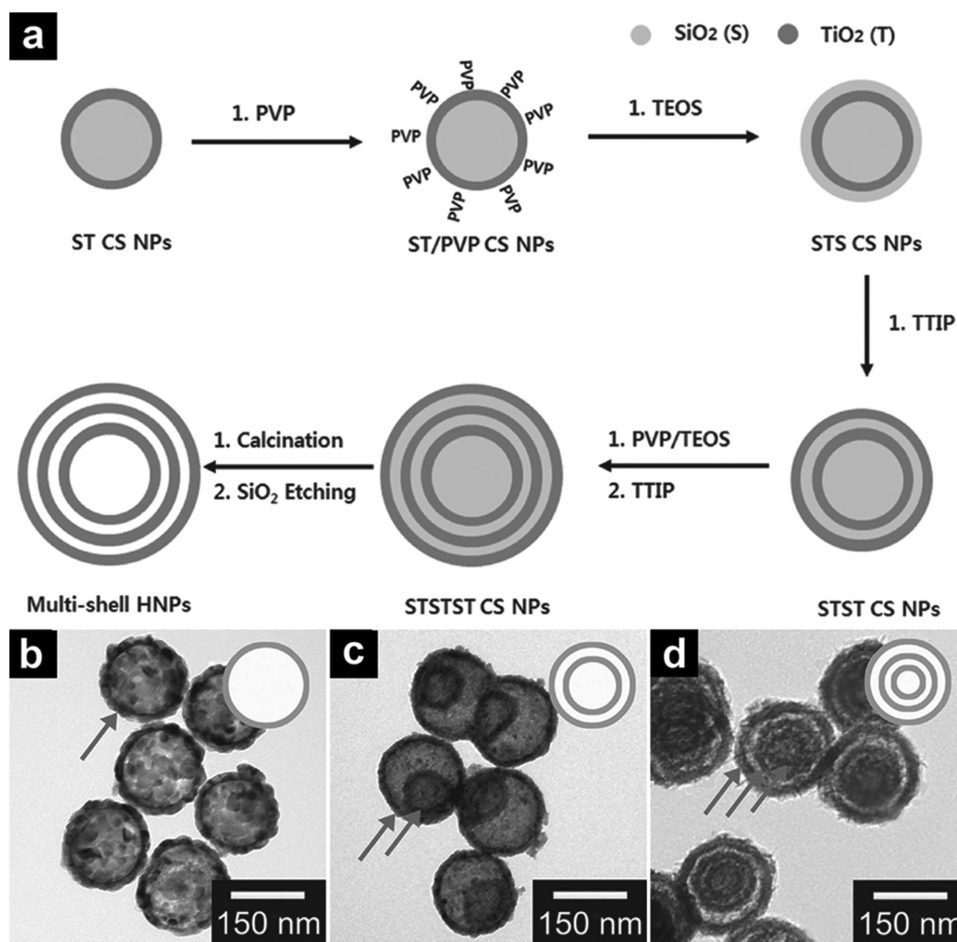


Figure 1. a) Schematic illustration for the hard templating synthesis of TiO₂ TSHSs. b–d) TEM images of TiO₂ SSHSs (b), DSHSs (c), and TSHSs (d). Reproduced with permission.^[25]

SiO₂@TiO₂@SiO₂@TiO₂@SiO₂@TiO₂ core–shell spheres via sol–gel processes. After calcination and NaOH etching, TiO₂ single-shelled hollow spheres (SSHs) (Figure 1b), double-shelled hollow spheres (DSHSs) (Figure 1c), and triple-shelled hollow spheres (TSHSs) (Figure 1d) can be obtained. By a similar approach, the same group also prepared SiO₂/TiO₂ SSHSs and DSHSs.^[26,27] In the latter case, a mild etchant (NH₃·H₂O), rather than NaOH, is used to partially dissolve the SiO₂ core and sacrificial layer.

Li et al. reported the preparation of nearly monodisperse poly(methacrylic acid) (PMAA) double-shelled hollow spheres and SiO₂ core-in-double-shell hollow spheres via hard templating.^[28] Alternating SiO₂@PMMA tetra- and penta-layered hybrid spheres are first prepared by combining the sol–gel process and distillation–precipitation polymerization. Etching the SiO₂ from the SiO₂@PMMA@SiO₂@PMMA tetra-layer spheres with HF generates double-shelled PMAA hollow spheres. On the other hand, removal of the PMAA layers from the SiO₂@PMMA@SiO₂@PMMA@SiO₂ penta-layered spheres by calcination produces SiO₂ core-in-double-shell hollow spheres. Similarly, Cao et al. reported the fabrication of monodisperse double-shelled SiO₂ hollow spheres using cationic poly(styrene) (CPS) particles as the hard templates.^[29]

The shell-by-shell deposition of target materials and sacrificial layers on hard templates is generally complex and tedious, making the low cost and scalable production of MSHSs unfeasible. As a result, tremendous efforts have been dedicated to simplifying the hard-templating process. Conventionally, the synthesis of a colloidal template, the deposition of target materials, and the coating of sacrificial layers are achieved under different synthetic conditions. If two or three of the above processes can be fulfilled under the same conditions, the synthesis of MSHSs can be significantly simplified. Stöber SiO₂ spheres, a widely employed hard template in hollow sphere synthesis, are usually synthesized by the hydrolysis and condensation of silicon alkoxide (e.g., tetraethyl orthosilicate (TEOS)) in a water/alcohol mixture (e.g., water/ethanol) in the presence of a base catalyst (e.g., ammonia).^[24] Interestingly, monodisperse resorcinol–formaldehyde (RF) resin spheres can be created through the polymerization of resorcinol and formaldehyde under the Stöber conditions (water–ethanol–ammonia) as well.^[30] This fact creates tremendous opportunities in the preparation of novel hollow structures. Fuertes et al. reported the one-step synthesis of SiO₂@RF core–shell spheres by the Stöber method.^[31] The SiO₂@RF core–shell structure is obtained because the hydrolysis and condensation of TEOS proceeds much quicker

than the polymerization of resorcinol and formaldehyde. RF polymeric hollow spheres can be generated by dissolving the SiO₂ core of the SiO₂@RF spheres; hollow carbon spheres can be obtained by carbonization of the SiO₂@RF followed by HF etching.

Yu and co-workers extended the Stöber method to the synthesis of a series of hollow carbon colloids, including intact SSHSs, intact DSHSs, invaginated (bowl-like) DSHSs, endo-invaginated DSHSs, intact TSHSs, and invaginated TSHSs.^[32] The synthesis is carried out under the Stöber conditions with TEOS, resorcinol, and formaldehyde as precursors (Figure 2). Due to the relatively fast hydrolysis and condensation rates of TEOS, Stöber SiO₂ spheres form first via homogeneous nucleation. The RF precursors preferentially polymerize on the SiO₂ surface through heterogeneous nucleation (step I). For the synthesis of DSHSs, TEOS is introduced for the second time at a chosen time point (step II). The subsequent heterogeneous nucleation of SiO₂ leads to the formation of uniformly

distributed SiO₂ islands on the RF shell. The residual RF oligomers co-condense with the SiO₂ nanoparticles to form a composite SiO₂/RF layer. After carbonization (step III) and SiO₂ removal (step IV), DSHSs are obtained. By controlling the thickness of the carbon shells or the size of the SiO₂ islands, the morphology of the DSHSs can be finely regulated from intact spheres to invaginated spheres or endo-invaginated spheres. With a similar strategy, Zang et al. obtained single-shelled and double-shelled mesoporous carbon hollow spheres by introducing the cationic surfactant cetyltrimethyl ammonium bromide (CTAB) into the synthesis.^[33]

In some cases, it is found that the shell-by-shell deposition of target materials on a hard template can also lead to MSHSs, while no sacrificial layer is required. As a specific example, Lou et al. developed a hydrothermal shell-by-shell deposition method for the preparation of nearly monodisperse SnO₂ hollow spheres with a single (Figure 3a) or a double shell.^[34] In this novel approach, SiO₂ spheres are used as the hard

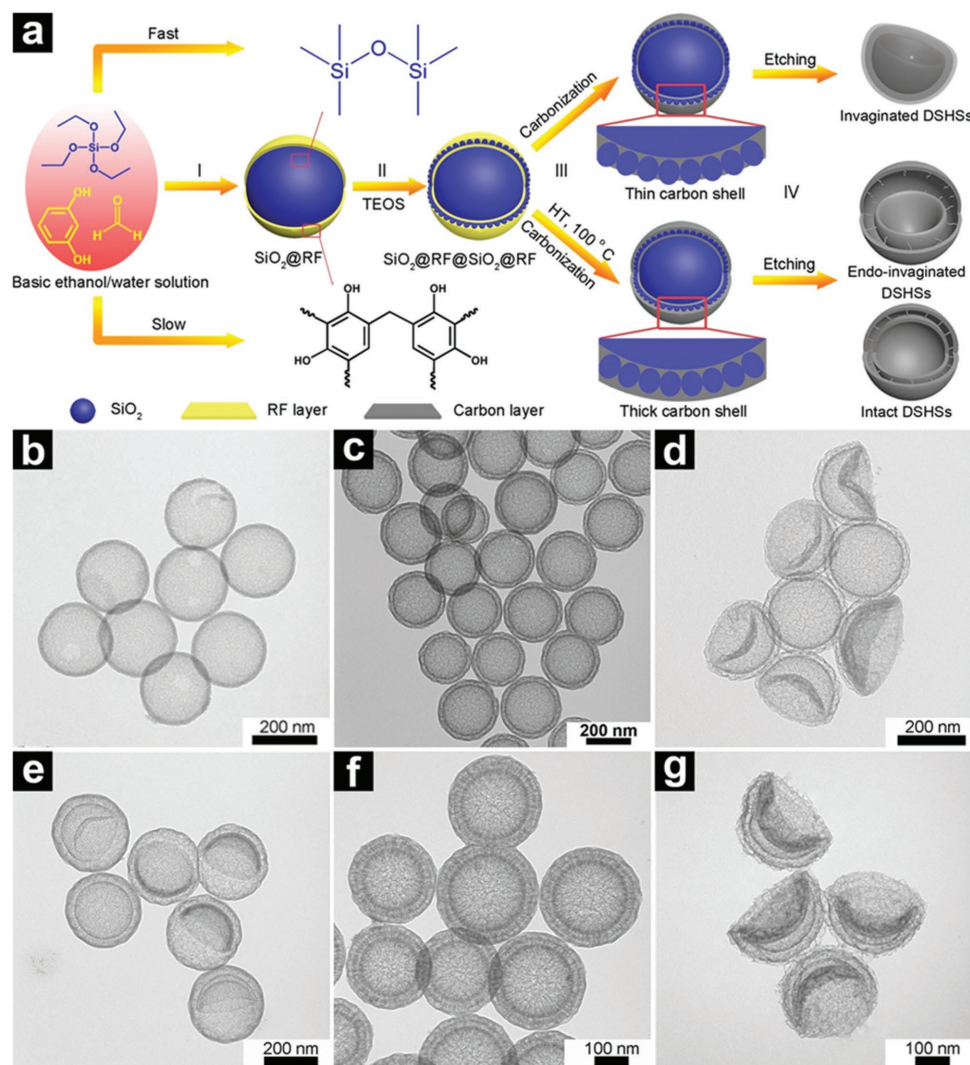


Figure 2. a) Schematic illustration for the synthesis of invaginated, endo-invaginated, and intact DSHSs. b–g) TEM images of intact SSHSs (b), intact DSHSs (c), invaginated DSHSs (d), endo-invaginated DSHSs (e), intact TSHSs (f), and invaginated TSHSs (g). Reproduced with permission.^[32] Copyright 2015, American Chemical Society.

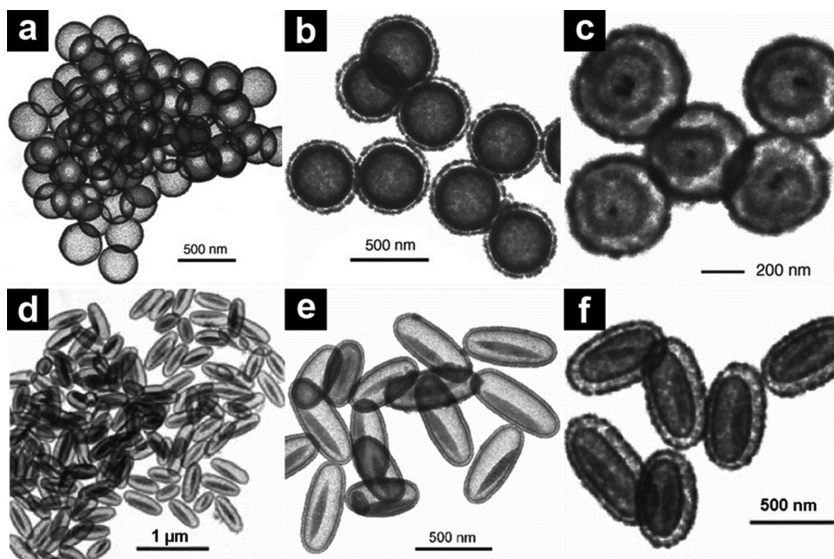


Figure 3. a–f) TEM images of SnO₂ SHHSs (a), SnO₂ DSHSs obtained from one-step hydrothermal deposition (b), Au@SnO₂ DSHSs (c), single-walled SnO₂ nanococoons with movable α -Fe₂O₃ spindles (d), double-walled SnO₂ nanococoons with movable α -Fe₂O₃ spindles obtained from repeated hydrothermal shell-by-shell deposition (e), and double-walled SnO₂ nanococoons with movable α -Fe₂O₃ spindles obtained from one-step hydrothermal deposition (f). a–c) Reproduced with permission.^[34] d–f) Reproduced with permission.^[36]

templates; and polycrystalline SnO₂ can be hydrothermally deposited on the surface of SiO₂ to form a uniform single shell. A second shell can be created by simply repeating the hydrothermal deposition process (the so-called shell-by-shell deposition). Interestingly, by controlling the relative amount of SiO₂ template, it is also possible to create SnO₂ DSHSs via a one-step hydrothermal deposition (Figure 3b). This hydrothermal deposition method requires no prior surface modification, which may benefit from the compatibility between the SiO₂ templates and polycrystalline SnO₂. Another advantage of this approach is that functional components, such as Au nanoparticles (Figure 3c)^[34] and Fe₃O₄ magnetic particles,^[35] can be easily introduced in the interior cavity of the SnO₂ hollow spheres.

The power of the hydrothermal shell-by-shell deposition is further demonstrated by applying this method to non-spherical templates.^[36] The synthesis starts from coating hematite (α -Fe₂O₃) spindles with a SiO₂ layer using the Stöber process, which produces ellipsoidal α -Fe₂O₃@SiO₂ core-shell particles. The resultant α -Fe₂O₃@SiO₂ particles are then employed as the hard templates and subjected to hydrothermal shell-by-shell deposition. Single-step and repeated hydrothermal deposition leads to single-walled (Figure 3d) and double-walled (Figure 3e) SnO₂ nanococoons with movable α -Fe₂O₃ spindles after SiO₂ removal. As in the case of spherical SiO₂ templates, double-walled hollow structures (Figure 3f) can be achieved via single-step hydrothermal deposition if the amount of template is reduced.

2.1.2. Templating Against Porous Hollow Structures

Besides solid colloids, porous hollow structures can also be employed as the hard templates for the fabrication of MSHSs. Contrary to solid templates, the desired materials can be coated on both the exterior and interior surfaces of the porous hollow structures. As a result, double-shelled hollow structures can be achieved with one target-material-coating–template-removal cycle. For example, Yang et al. reported a general synthetic route toward DSHSs using hollow latex spheres as the templates.^[37] The synthesis begins with the sulfonation of commercially available polystyrene (PS) hollow spheres (Figure 4a). The sulfonation process functionalizes the exterior surface, the interior surface, and the transverse channels of the PS hollow spheres with hydrophilic sulfonic acid groups ($-\text{SO}_3^-\text{H}^+$). Immersion of the sulfonated PS hollow spheres into a tetrabutyl titanate sol generates sandwich-structured TiO₂@PS@TiO₂ hollow spheres. Selective removal of the PS by a suitable solvent or calcination leads

to the formation of TiO₂ DSHSs (Figure 4b,c). The sulfonation time determines the thickness of the sulfonated hydrophilic shell and thus the thickness of the target hollow spheres. As the sulfonic acid groups is capable of interacting with a large variety of species, such as metal ions (e.g., Fe³⁺), metal oxide precursors (e.g., titanium alkoxides), and basic organic molecules (e.g., aniline), various functional components can be deposited on the sulfonated hydrophilic locations of the template. Besides TiO₂ DSHSs, Fe₃O₄ and polyaniline, DSHSs can also be produced by this method. With a modified approach, the same group deposited TiO₂ and SiO₂ on the interior and

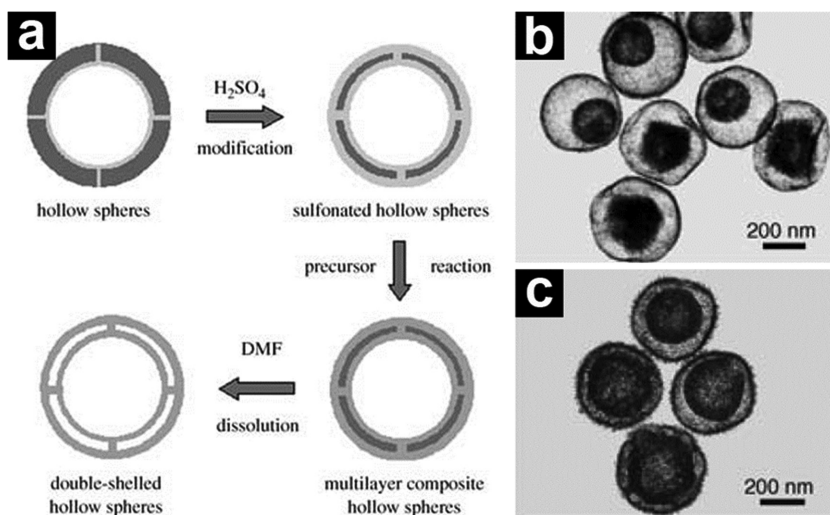


Figure 4. a) Schematic illustration for the formation of DSHSs using PS hollow spheres as the hard templates. b,c) TEM images of TiO₂ DSHSs with thin (b) and thick shells (c). Reproduced with permission.^[37]

exterior surfaces of the hollow PS spheres, respectively. After removing the PS interlayer, double-shelled composite hollow spheres were obtained; the inner shell was composed of TiO_2 , while the outer shell was composed of SiO_2 .^[38]

Lou, Guo, and co-workers reported the fabrication of double-shelled hollow carbon spheres, using porous SnO_2 hollow spheres as the hard templates.^[39] The synthesis involves: i) preparation of porous SnO_2 hollow spheres, ii) coating the porous SnO_2 hollow spheres with glucose-derived polysaccharide on the exterior/interior surfaces and in the pores of the shell, iii) carbonization, and iv) template removal. By employing Fe_3O_4 porous hollow spheres as the templates and a similar coating approach, Qian and co-workers fabricated pristine and N-doped double-shelled hollow carbon spheres.^[40] The N-doping is achieved by HNO_3 treatment of the Fe_3O_4 @C precursors. Using TiO_2 hollow spheres as the hard templates and dopamine as the N-containing carbon precursor, Manthiram and co-workers prepared N-doped double-shelled hollow carbon spheres.^[41] The TiO_2 hollow spheres possess a porous shell, through which the dopamine molecules penetrate into the hollow interior. The dopamine polymerizes, forming a polydopamine coating on the exterior/interior surfaces and in the pores of the TiO_2 shell. N-doped double-shelled hollow carbon spheres can be obtained after carbonization and HF etching. Pang et al. prepared double-shelled poly(3,4-ethylenedioxythiophene) (PEDOT) and polypyrrole (PPy) hollow spheres using Fe_3O_4 hollow spheres as sacrificial templates.^[42] Besides hollow spheres, Fe_3O_4 yolk-shell structures can also be employed as the sacrificial templates. In this case, the exterior surface of the shell and the interior surface of the shell, as well as the surface of the core can be coated with conducting polymers, and triple-shelled PEDOT hollow spheres can be obtained after template removal. By judicious selection of the template, even more complex MSHSs can be achieved. For example, Song, Gao and co-workers constructed double- and quadruple-shelled hollow carbon spheres by employing single- and double-shelled mesoporous-silica hollow spheres as the templates.^[43]

2.2. Soft Templating

Amphiphilic molecules such as surfactants and block copolymers are able to self-assemble into micelles or vesicles with different structures when their concentration in solution exceeds the critical micelle concentration (CMC).^[2] Such micelles and vesicles can act as soft templates directing the formation of hollow structures. However, the micelles and vesicles are thermodynamically metastable, and they are very sensitive to the synthesis parameters, such as temperature, pH value, concentration of the amphiphilic molecules, solvent, organic/inorganic additives, and ionic strength of the solution. In principle, this sensitivity can provide delicate control over the morphology and structure of the micelle/vesicle template. In practice, however, it makes the widespread application of micelle/vesicle templating in constructing hollow structures with various compositions and morphologies difficult, as the addition of target precursors into the synthesis system may affect the micelle/vesicle formation.

Despite it being challenging, a variety of inorganic materials with MSHS have been prepared by micelle/vesicle templating. Among these materials, silica and silica-based hybrid materials are no doubt the most successful examples due to the well-controlled hydrolysis and condensation behaviors of silica precursors in aqueous solution. Pinnavaia and co-workers reported the synthesis of ultrastable mesostructured silica vesicles with the shells constructed of one or more undulated silica sheets through a supramolecular assembly pathway.^[44] The hydrogen bonding between electrically neutral gemini surfactants ($\text{C}_n\text{H}_{2n+1}\text{NH}(\text{CH}_2)_2\text{NH}_2$) and silica precursors derived from TEOS play a significant role in the assembly. Liu et al. prepared multishelled mesoporous-silica hollow spheres with uniform size, tunable shell thickness, and controlled shell number (1 to 4 shells) through vesicle templating using $[\text{C}_3\text{F}_7\text{O}(\text{CFCF}_3\text{CF}_2\text{O})_2\text{CFCF}_3\text{CONH}(\text{CH}_2)_3\text{N}^+(\text{C}_2\text{H}_5)_2\text{CH}_3\text{I}^-]$ (FC4) and $\text{EO}_{106}\text{PO}_{70}\text{EO}_{106}$ (F127) as the soft templates.^[45] Zhang et al. reported the high yield synthesis of organosiliceous multilamellar vesicles through a single-surfactant vesicle-templating approach using Pluronic P85 as the structure-directing agent and 1,2-bis(triethoxysilyl)ethane (BTEE) as the organosilica precursor.^[46]

The polymerization of phenol and formaldehyde can be well controlled in solution, and the resulting polymer (phenolic resin) possesses a three-dimensional (3D) covalently bonded framework like that of amorphous silica. Both factors inspire the extension of soft templating to the synthesis of phenolic resin multilayer vesicles. Gu et al. first reported the synthesis of mesoporous phenolic-resin-silica multilayer vesicles through an aqueous emulsion coassembly approach.^[47] In this multiconstituent coassembly, a low-molecular-weight water-soluble resol, prehydrolyzed TEOS, commercially available Pluronic F127, and 1,3,5-trimethylbenzene (TMB) were selected as the carbon precursor, silica source, soft template, and organic co-solvent, respectively. The as-synthesized phenolic-resin-silica multilayer vesicles had 3–9 shells. Calcination at 350 °C in N_2 removes the template; further carbonization at 900 °C affords mesoporous-carbon-silica multilayer vesicles with carbon pillars located between the layers to stabilize the lamellar structure. Etching of silica yields mesoporous-carbon multilayer vesicles, while calcination in air or microwave digesting removes the organic components and results in mesoporous-silica vesicles. Liu et al. reported the preparation of multilayered mesoporous resorcinol-formaldehyde hollow spheres with concave surface via organic-organic self-assembly in acidic ethanol/water solution.^[48] Multilayered mesoporous-carbon hollow spheres with a concave surface can be obtained by carbonization of the corresponding polymer spheres.

Besides silica- and carbon-based materials, the micelle/vesicle templating can also be applied to the synthesis of MSHSs with other compositions, such as TMOs. Wang and co-workers reported the vesicle-templating synthesis of single-crystalline Cu_2O hollow spheres by using CTAB as the template (Figure 5) in aqueous solution.^[49,50] By fine adjustment of the concentration of CTAB (from 0.10 to 0.15 M), the structure of the Cu_2O hollow spheres can be tuned from single- to double-, triple-, and quadruple-shelled. Similarly, Ma, Yao and co-workers reported the synthesis of Co_3O_4 SSHSs, DSHSs, and TSHSs by employing poly(vinylpyrrolidone) (PVP) as a soft template.^[51]

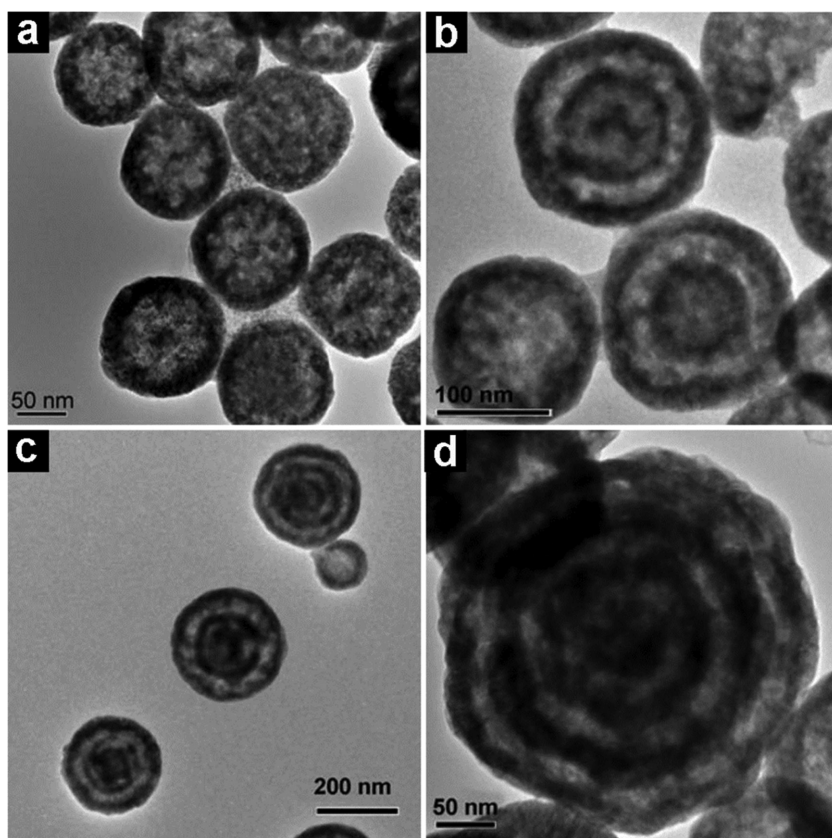


Figure 5. a–d) TEM images of single-shelled (a), double-shelled (b), triple-shelled (c), and quadruple-shelled (d) Cu_2O hollow spheres. Reproduced with permission.^[49]

An interesting feature of these hollow spheres are that they are constructed from nanosheet building blocks. It is speculated that PVP multilamellar vesicles with controlled shell numbers form at first. Due to the strong coordination interaction between the functional groups on PVP (–N and C=O groups) and metal ions, the cobalt glycolate oligomers preferentially deposit on the multishells of the PVP vesicles. Co_3O_4 multishelled hollow spheres can be obtained after template removal. As in the case of Cu_2O hollow spheres, the shell number of Co_3O_4 hollow spheres is also dependent on the concentration of surfactant; increase in PVP concentration leads to increased shell numbers. This method is then extended to the preparation of Co_3O_4 – Fe_3O_4 multishelled hollow spheres.^[52]

2.3. Selective Etching of “Soft@Hard” Particles

Etching has been widely employed in removal of templates and sacrificial interlayers during the fabrication of hollow structures. The composition of templates and sacrificial interlayers is usually different from that of the desired material. Recently, it has been demonstrated that the creation of hollow structures through selective etching of a single-component material, such as SiO_2 , Prussian Blue (PB), $\text{ZnSn}(\text{OH})_6$, and $\text{CoSn}(\text{OH})_6$, is also possible. A common feature of these parent materials is that they all have some “soft regions” and “hard regions”.

Stöber SiO_2 spheres are perceived to be “homogeneous” in nature and uniform under microscopy. However, some recent reports have revealed that some regions of the Stöber SiO_2 spheres and their derivatives might be selectively etched away by HF, NaOH, $\text{NH}_3 \cdot \text{H}_2\text{O}$, Na_2CO_3 , or hot water, generating yolk–shell and hollow structures.^[53–57] Chen et al. unambiguously demonstrated that the selectivity in etching originated from the inhomogeneous nature of the Stöber SiO_2 spheres.^[58] Under Stöber synthetic conditions, TEOS undergoes stepwise hydrolysis, producing incompletely and completely hydrolyzed monomers with 1–4 hydroxyl groups. The further and simultaneous condensation of these monomers results in the formation of Stöber SiO_2 spheres. Given the slow hydrolysis rate of TEOS, a gradient in condensation degree and chemical stability is expected in the resultant SiO_2 spheres. The innermost region formed at the early stages contains a high fraction of uncondensed ethoxy groups. As a result, this region has a low crosslinking degree and thus low chemical stability (defined as “soft”). The outermost layer formed at the later stages, in contrast, has a high crosslinking degree and high chemical stability (defined as “hard”), as it is mostly derived from the condensation of silicic acid. The unstable “soft region” can be stabilized with some post-treatment such as incubation. With this new understanding,

multishelled $\text{Au}@\text{SiO}_2$ yolk–shell structures can be fabricated by repeated SiO_2 deposition–incubation–hot-water-etching, which is quite facile and reproducible.

Just like the Stöber SiO_2 spheres, periodic mesoporous organosilica (PMO) spheres prepared by the Stöber method are also inhomogeneous in condensation degree and stability. Taking full advantage of the inhomogeneous nature of the PMO spheres and selective etching, Zhao, Lu and co-workers extended the above concept to the fabrication of PMO multishelled hollow spheres (Figure 6).^[59] As shown in Figure 6a, mesostructured ethane-bridged organosilica spheres were first prepared by a modified Stöber method using CTAB as the soft templates, and 1,2-bis(triethoxysilyl)ethane (BTSE) and TEOS as the precursors. Repeated addition of BTSE and TEOS generated multilayered organosilica/CTAB composite spheres with increased diameter. As in the case of Stöber SiO_2 spheres, the inner regions of each organosilica layer formed at the early stages of reaction were relatively “soft” with a low condensation degree, while the outer regions of each layer formed at the later stages of the reaction were relatively “hard” with a high condensation degree. When the as-obtained organosilica/CTAB spheres were subjected to hydrothermal treatment, the inner regions (“soft regions”) of each organosilica layer were attacked by the water and dissolved, while the outer regions (“hard regions”) of each layer persisted and formed multiple hollow shells (Figure 6b). After extraction of the CTAB, PMO

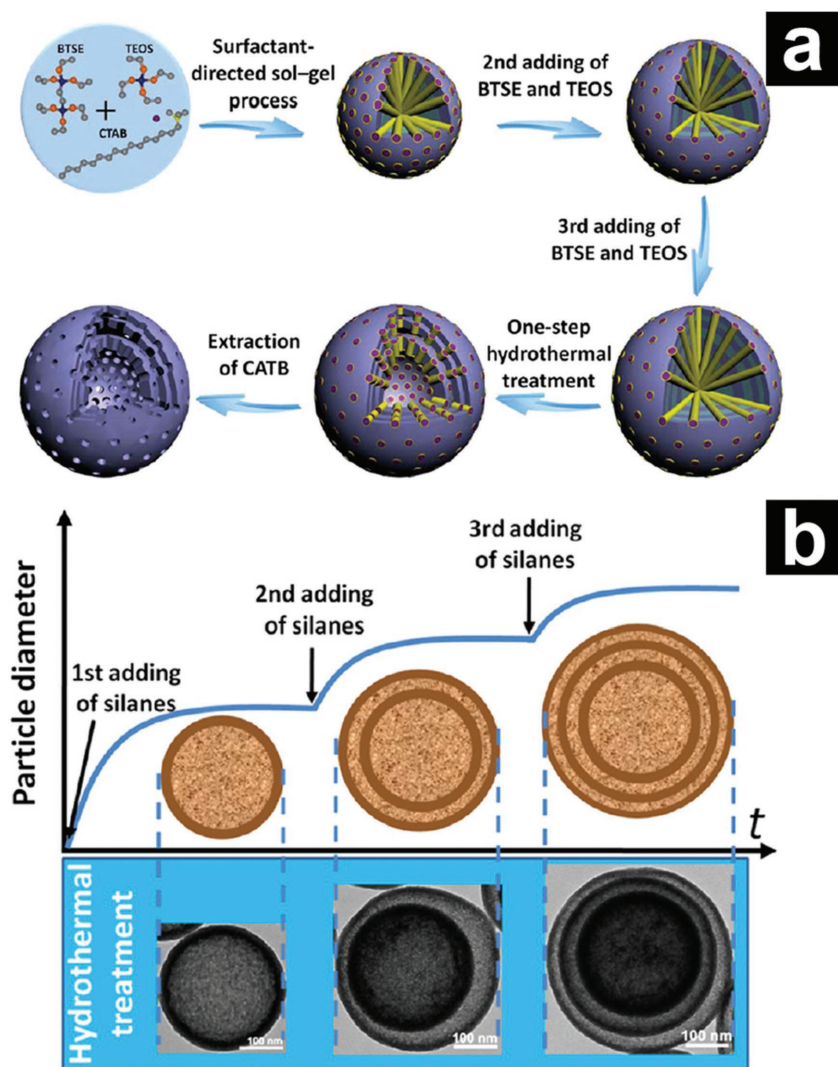


Figure 6. a,b) Schematic illustration for the preparation of triple-shelled PMO hollow spheres (a) and schematic illustration for the successive growth process of the organosilica/CTAB composite spheres under Stöber conditions and the corresponding multishelled PMO hollow spheres after hydrothermally induced selective etching (b). Reproduced with permission.^[59] Copyright 2015, American Chemical Society.

multishelled hollow spheres with ordered mesoporous channels could be obtained. The number of shells could be easily controlled by the addition time of silane precursors. The overall diameter, intershell spacing, and shell thickness of the PMO multishelled hollow spheres could be precisely modulated by tuning the CTAB concentration, the amount of organosilica cores, and the reaction temperature, respectively. Another salient feature of this approach is that different shells of the PMO multishelled hollow spheres can be functionalized with different organic groups, endowing the products with multiple functions. More examples of SiO_2 - and PMO-based multishelled hollow spheres prepared via selective etching have been reported by Yeh and co-workers^[60] and Tang and co-workers.^[61]

Apart from SiO_2 and its derivatives, the selective etching strategy can also be applied to the preparation of intricate hollow structures with other compositions. For example, the

core of $\text{ZnSn}(\text{OH})_6$ and $\text{CoSn}(\text{OH})_6$ nanocubes can be selectively etched by NaOH , generating porous and single-crystalline $\text{ZnSn}(\text{OH})_6$ and $\text{CoSn}(\text{OH})_6$ nanoboxes.^[62,63] By combining repeated deposition of $\text{CoSn}(\text{OH})_6$ onto pre-grown seeds (such as nanocubes and nanoboxes) and subsequent alkaline etching, a series of $\text{CoSn}(\text{OH})_6$ complex hollow structures can be fabricated, including yolk-shell cubes and double-, triple-, and quadruple-shelled nanoboxes. This approach can be easily extended to the fabrication of $\text{ZnSn}(\text{OH})_6$ MSHSs, which can then be converted into ZnSnO_3 and $\text{Zn}_2\text{SnO}_4/\text{SnO}_2$ MSHSs.^[64,65] Interestingly, even single-crystalline PB mesocrystals can also be considered as “soft@hard” particles. They possess more defects and lower stability in the core region, while having fewer defects and higher stability at the outermost region. As such, the “soft” cores of PB can be selectively etched by hot HCl in the presence of PVP, leaving behind “hard” hollow shells.^[66] The “soft@hard” PB crystals can be used as the seed for further crystal growth, generating “soft@hard@soft@hard” PB particles. When the “soft@hard@soft@hard” PB particles are immersed in an acidic solution, the “soft regions” can be selectively removed, while the “hard regions” can be preserved, resulting in double-shelled PB hollow structures.^[67] This concept can be further applied to the preparation of yolk-shell and core-in-double-shell hollow structures of PB analogues.

2.4. Ostwald Ripening

Ostwald ripening is a well-known phenomenon in crystal growth.^[68] According to the IUPAC definition, it refers to the “dissolution of small crystals or sol particles and the re-deposition of the dissolved species on the surfaces of larger crystals or sol particles”. Over a decade ago, Yang and Zeng first demonstrated the Ostwald ripening mechanism as a template-free route for the preparation of SSHSs.^[69] Primary TiO_2 crystallites are first generated through the hydrolysis of TiF_4 under hydrothermal conditions. To minimize the total interfacial energy, the TiO_2 crystallites aggregate into spherical assemblies. The inner crystallites formed in the early stages of nucleation and crystal growth are relatively small and have high surface energies, while those in the outer surfaces formed in the later stages are relatively large. As a result, the central region of the spheres begins to evacuate through dissolution, generating a hollow cavity.

Recently, Ostwald ripening has been further proven to be an efficient process in constructing MSHSs. For example, Zhang and Wang developed a multistep Ostwald ripening approach for the geometry-controlled fabrication of Cu_2O

multishelled hollow spheres.^[70] The first Ostwald ripening process generates Cu₂O SSHSs. With the introduction of additional reactants into the reaction mixture, new Cu₂O crystallites are produced; the newly generated Cu₂O is deposited on the surface of the first shell, forming a thicker shell with an increased overall diameter. During the second Ostwald ripening process, the freshly formed crystallites with relatively small crystallite size (attached to the first shell originally) evacuate, while the freshly formed crystallites with relatively large crystallite size survive (located at the outmost surface), leading to the formation of Cu₂O DSHSs. Triple-shelled and quadruple-shelled Cu₂O hollow spheres can also be easily prepared by repeating the deposition-then-ripening cycle.

To further increase the architectural complexity and flexibility, Yec and Zeng developed a seed-mediated-growth-successive-Ostwald-ripening strategy to fabricate a family of Cu₂O(@Cu₂O)_n (*n* = 1–4) multishelled core-shell and yolk-shell structures (Figure 7).^[71] Single-crystalline Cu₂O nanocubes (type A) with the ability to withstand multiple Ostwald ripening processes are employed as the original seeds. The Cu₂O seeds are then added to a nutrient solution and subjected to seed-mediated-growth-Ostwald-ripening process for shell growth. After one growth-ripening cycle, either a concentric Cu₂O@Cu₂O core-shell structure (type B) or an eccentric Cu₂O@Cu₂O yolk-shell structure (type C) can be obtained. Interestingly, the core-shell and yolk-shell structures obtained from a previous step can serve as newer-generation seeds for subsequent shell growth, resulting in structures with even more complex configurations and architectures. In addition,

the centricity and eccentricity of the core-shell and yolk-shell structures can be controlled at each growth-ripening cycle. With two growth-ripening cycles, double-shelled structures with four configurations can be obtained (types D to G); with three growth-ripening cycles, triple-shelled structures with eight configurations can be obtained (types H to O). By tuning the synthetic parameters, connecting individual multishelled spheres into bean-pod like structures is also possible (types R to U). A total of 20 representative structures have been synthesized using this strategy.

It should be pointed out that, if we define the small crystallites with high surface energy as “soft regions” and the large crystallites with low surface energy as “hard regions”, Ostwald ripening can be regarded as a selective etching process of “soft@hard” particles as well. The only difference is the “soft” small crystallites dissolved in solution can be re-deposited as “hard” large crystallites on the surface.

2.5. Ion Exchange

Ion exchange is the process in which ions (either cations or anions) are exchanged between a solution and an insoluble solid. It has been widely employed in purification, separation, and water decontamination. Recently, ion exchange has been exploited as a powerful method for the fabrication of hollow structures, including MSHSs. As a successful example, Xiong and Zeng reported the fabrication of single-, double-, triple-, and quadruple-shelled Cu₂S hollow spheres through a serial ion-exchange approach using Cu₂O–PVP hybrid colloids as

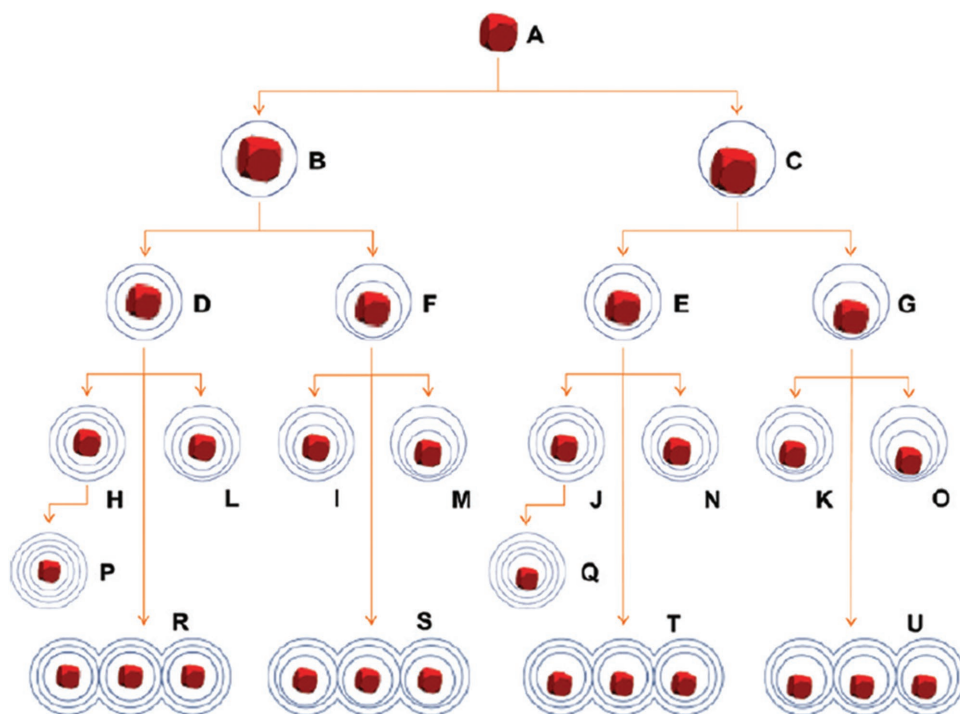


Figure 7. Schematic illustration for the synthesis of a family of Cu₂O(@Cu₂O)_n (*n* = 1–4) core-shell and yolk-shell structures (B to U) by a seed-mediated-growth-successive-Ostwald-ripening strategy. The red cubes represent single-crystalline Cu₂O seeds, while the blue circles represent polycrystalline Cu₂O shells. Reproduced with permission.^[71] Copyright 2012, American Chemical Society.

the precursors (Figure 8).^[72] The Cu_2O -PVP precursor spheres are synthesized with a PVP-assisted polyol method (step 1). During the ion exchange, the S^{2-} ions released from thiourea react with the Cu_2O and produce a Cu_2S surface layer (step 2). Due to the fast outward diffusion of O^{2-} and slow inward diffusion of S^{2-} , a gap is developed between the Cu_2O core and Cu_2S shell (step 3). The Cu_2S surface layer formation (on the inner Cu_2O core) and gap development processes can be repeated several times (steps 4 to 9), and the second, third, and fourth Cu_2S shell are produced sequentially.

As another example, Shen et al. extended the ion-exchange strategy for the fabrication of ternary metal sulfide (NiCo_2S_4) DSHSs (Figure 9).^[73] In this approach, uniform nickel cobalt glycerate (NiCo -glycerate) spheres prepared by a facile solvothermal method are used as the precursor (Figure 9b). The NiCo -glycerate precursor spheres are then subjected to a solution-sulfidation process to convert the glycerate into sulfide and induce the solid-to-hollow transformation. The sulfidation process can be divided into three stages. At stage I, S^{2-} ions are released from thioacetamide at a high temperature. The S^{2-} ions can then react with the NiCo -glycerate spheres, producing NiCo -glycerate@ NiCo_2S_4 core-shell spheres (Figure 9c). Due to the slow inward diffusion of S^{2-} ions and fast outward diffusion of metal ions, a well-defined gap between the glycerate core and sulfide shell is developed with continuous reaction (stage II, Figure 9d). With a gap between the core and shell, the outward diffusion of metal ions is blocked, while the inward diffusion of S^{2-} ions is not affected or even facilitated. As a result, a second NiCo_2S_4 shell is formed on the inner glycerate core. As the sulfidation goes on, NiCo_2S_4 DSHSs are finally obtained (stage III, Figure 9e). By adjusting the synthesis conditions, such as reaction temperature, NiCo_2S_4 yolk-shell structures and SSHSs can also be obtained. Apart from NiCo_2S_4 , MnCo_2S_4 DSHSs can also be created by using MnCo -glycerate spheres as the precursor, demonstrating the versatility of this approach.

2.6. Thermally Induced Matter Relocation

Matter relocation plays a significant role in Ostwald ripening,^[69,70] ion exchange,^[71,72] and the Kirkendall effect,^[74,75] three widely studied mechanisms for the construction of hollow structure. Recently, it has been found that the thermal decomposition of a series of materials may lead to the formation of either simple or complex hollow structures, during which thermally induced matter relocation plays an indispensable role. These materials include metal carbonates,^[76] metal-organic frameworks (MOFs),^[77] metal glycolates,^[78] metal glycerates,^[79] metal-ion-containing carbon spheres,^[80]

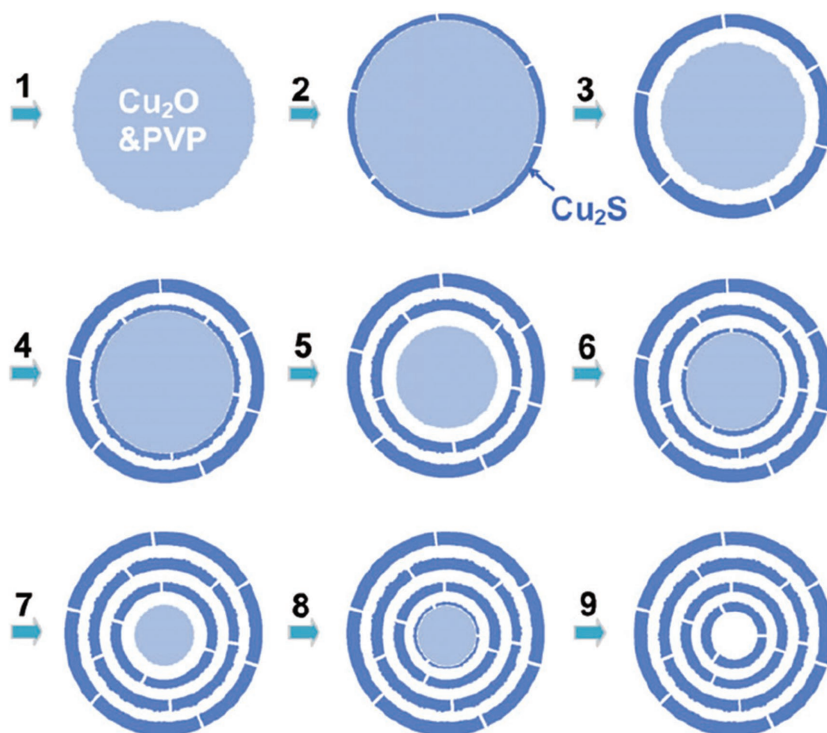


Figure 8. Schematic illustration for the formation of Cu_2S multishell hollow spheres. Step 1, preparation of Cu_2S -PVP hybrid spheres; step 2, surface Cu_2S formation through ion exchange; step 3, formation of the first shell; step 4, step 6, and step 8, Cu_2S formation on the inner Cu_2O core; step 5, step 7, and step 9 formation of the second, third, and fourth shell, respectively. Reproduced with permission.^[72]

metal-ion-/metal-oxide-containing polymer spheres,^[22,81] and metal-salt-organic-hybrid spheres.^[82] These materials share some similarities. First, they are composed of a metallic moiety and a decomposable organic/inorganic moiety. In most cases, the metallic moiety is dispersed homogeneously in the decomposable organic/inorganic matrix at atomic scale or the nanoscale. Second, they all experience significant weight loss during thermal decomposition in air due to the burn-off of the organic moiety and the release of gases. Third, for all these materials, matter relocation takes place during the thermal decomposition. Due to the above-mentioned similarities, a versatile hollow-structure-formation mechanism during thermal decomposition is expected.

Guan et al. proposed a non-equilibrium heat-treatment-induced heterogeneous contraction mechanism to explain the formation of a series of maghemite ($\gamma\text{-Fe}_2\text{O}_3$) hollow structures during the thermal decomposition of iron citrate-PVP gel spheres in air.^[81] They found that the structure of the products can be modulated from solid spheres to SSHSs, yolk-shell spheres, DSHSs, and core-in-double-shell hollow spheres by simply adjusting the heating rate (Figure 10). With a low heating rate of $1\text{ }^\circ\text{C min}^{-1}$, the gel spheres are almost homogeneously heated from the outermost surface to the center. As a result, $\gamma\text{-Fe}_2\text{O}_3$ solid spheres (A) are obtained. With a high heating rate of $10\text{--}250\text{ }^\circ\text{C min}^{-1}$, a temperature gradient (ΔT) along the radial direction of the gel spheres is expected. Due to the existence of ΔT , the outermost surface of the gel spheres

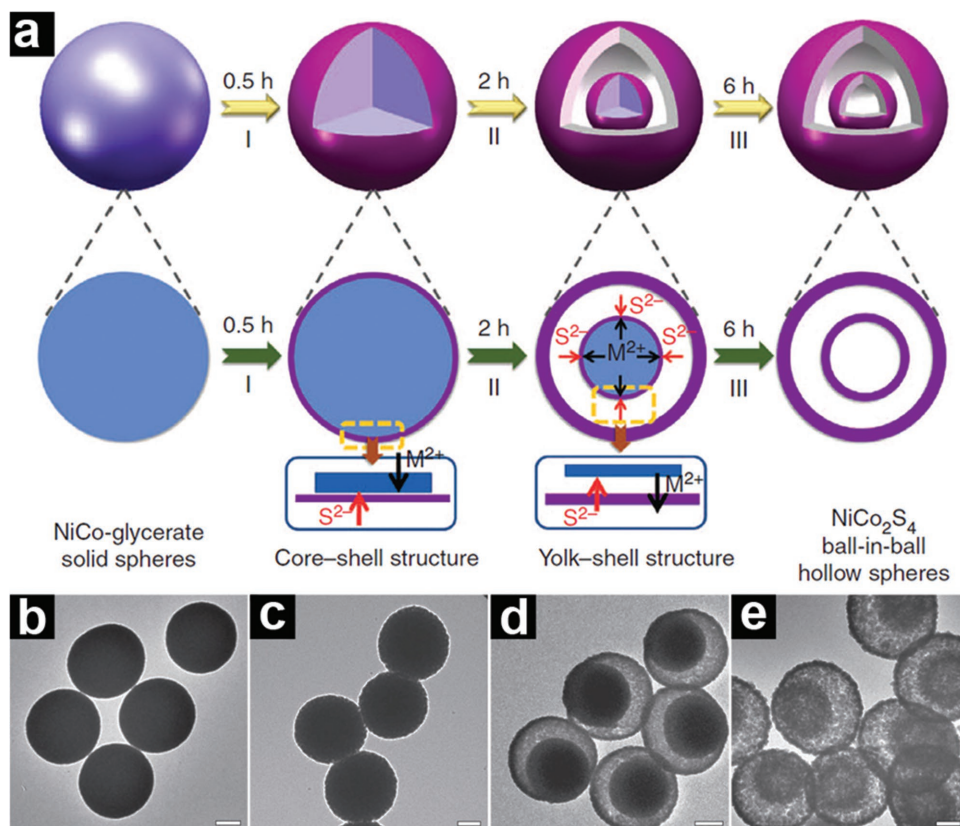


Figure 9. a) Schematic illustration for the formation of NiCo_2S_4 DSHSs. Stage I: surface NiCo_2S_4 formation via ion exchange. Stage II: formation of the first NiCo_2S_4 shell and formation of NiCo_2S_4 on the inner NiCo -glycerate core through S^{2-} diffusion. Stage III: completion of the ion-exchange reaction. M^{2+} refers to metal cations including Ni^{2+} and Co^{2+} . b–e) TEM images of the NiCo -glycerate precursor spheres (b), and the products after sulfidation of the NiCo -glycerate spheres for 0.5 h (c), 2 h (d), and 6 h (e). Scale bars in (b–e): 200 nm. Reproduced with permission.^[73] Copyright 2014, Nature Publishing Group.

decomposes first, forming an iron citrate–PVP@ $\gamma\text{-Fe}_2\text{O}_3$ core–shell structure. The $\gamma\text{-Fe}_2\text{O}_3$ shell is rigid; it can prevent the further contraction of the outer diameter. For the

iron citrate–PVP core, it continues to shrink due to the large weight loss in the subsequent annealing; that is to say, heterogeneous contraction happens. The interface between the iron citrate–PVP core and the $\gamma\text{-Fe}_2\text{O}_3$ shell experiences two forces of opposite direction: the cohesive force (σ_{co}) from the inner core and the adhesive (σ_{ad}) force from the rigid shell.

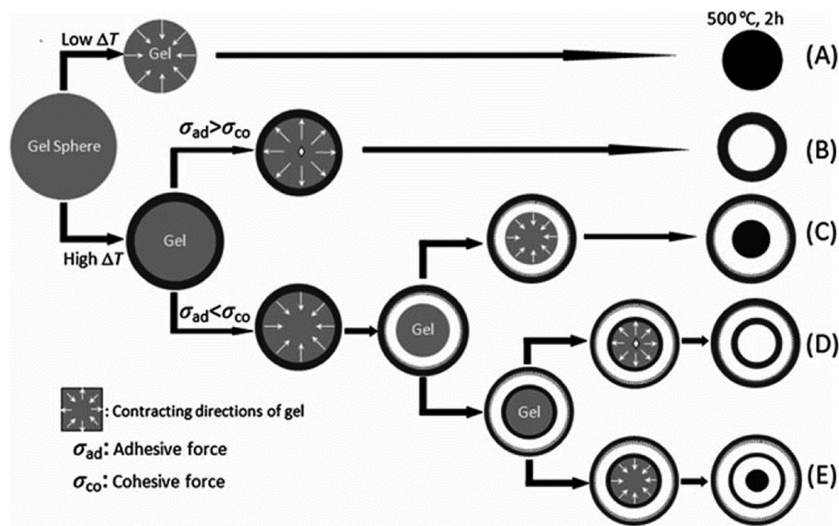


Figure 10. Schematic illustration for the formation of $\gamma\text{-Fe}_2\text{O}_3$ solid spheres (A), SSHSs (B), yolk–shell spheres (C), DSHSs (D), and core-in-double-shell hollow spheres (E) by sintering the iron citrate–PVP composite gel spheres at 500°C in air with different heating rates. Reproduced with permission.^[81] Copyright 2010, Royal Society of Chemistry.

The former promotes the inward shrinkage of the core, while the latter prevents the inward shrinkage. When $\sigma_{\text{co}} < \sigma_{\text{ad}}$, the inner core shrinks outward to the pre-formed shell, leading to the formation of $\gamma\text{-Fe}_2\text{O}_3$ SSHSs (B). This is what happens at a heating rate of $10^\circ\text{C min}^{-1}$. When the heating rate increases from 10 to $20^\circ\text{C min}^{-1}$, σ_{co} exceeds σ_{ad} . Therefore, the inner core contracts inwardly and separates from the rigid $\gamma\text{-Fe}_2\text{O}_3$ shell. For the as-generated core, the above formation processes of solid spheres or hollow spheres can be repeated depending on the remaining ΔT in the radial direction. The ΔT decreases with prolonged annealing time, as does σ_{co} . With a heating rate of $20^\circ\text{C min}^{-1}$, the remaining ΔT is too small to induce the formation of the second shell. As a result, the separated inner core shrinks

into a solid sphere, and yolk-shell structured are obtained (C). With a heating rate of $50\text{ }^{\circ}\text{C min}^{-1}$, the remaining ΔT is large enough to generate the second shell and DSHSs are achieved (D). With an even higher heating rate of $250\text{ }^{\circ}\text{C min}^{-1}$, the large remaining ΔT induces not only a second shell but also another inner core, resulting in the formation of core-in-double-shell hollow spheres (E). According to the non-equilibrium heat-treatment-induced heterogeneous contraction mechanism, even more complex hollow structures, such as triple-, quadruple-, and quintuple-shelled hollow spheres, can be expected if the ΔT is large enough. Although this mechanism was proposed for explaining the thermal decomposition behavior of iron citrate-PVP gel spheres, it can be generally applied to the thermal decomposition of other materials as well.

2.6.1. Thermal Decomposition of Metal Carbonates

Metal carbonates represent an important family of functional materials and minerals. They generally decompose on heating in air, generating the corresponding metal oxides and a significant amount of CO_2 and/or CO . Due to the non-equilibrium heat-treatment-induced heterogeneous contraction, various hollow structures may be formed during the thermal decomposition.^[76,83] For example, Zhou et al. designed double-shelled CoMn_2O_4 hollow microboxes through the thermal decomposition of $\text{Co}_{0.33}\text{Mn}_{0.67}\text{CO}_3$ microcubes (Figure 11), which were prepared by a simple co-precipitation method.^[76] Li and co-workers reported the synthesis of triple-shelled Mn_2O_3 hollow microcubes through a programmed annealing treatment.^[84] Qian and

co-workers fabricated double-shelled Mn_2O_3 hollow spheres by combining KMnO_4 oxidation, HCl etching, and thermal decomposition of MnCO_3 .^[85] By virtue of the facile synthesis procedure (precipitation-thermal decomposition), rich composition, and easy morphological control, the thermal decomposition of metal carbonates represents a quite promising approach for the low cost and mass production of metal oxide MSHSs.

2.6.2. Thermal Decomposition of MOFs

MOFs, also known as coordination polymers and coordination networks, are a class of crystalline and porous materials consisting of metal ions/clusters and polydentate organic ligands. MOFs are very appealing precursors for the construction of metal oxide hollow structures due to the virtually infinite combinations of metal ions and ligands, rich compositions, well-defined morphologies, and easy availability.^[77,86,87] Upon calcination in air, the organic moieties of MOFs burn off, leaving behind the corresponding metal oxides. Due to the thermally induced matter relocation during calcination, hollow-structured metal oxides with well-defined morphologies can be obtained. Oh et al. first reported the synthesis of ZnO and Co_3O_4 multishelled hollow spheres by thermal decomposition of zinc- and cobalt-ion-containing coordination polymer (metallo Schiff base) particles (Figure 12).^[77] By employing a cation-exchange reaction before the thermal decomposition, hybrid metal oxide (CuO/ZnO , $\text{Co}_3\text{O}_4/\text{ZnO}$, $\text{CuO}/\text{Co}_3\text{O}_4$, and $\text{NiO}/\text{Co}_3\text{O}_4$) multishelled hollow spheres can be obtained. Wang and co-workers successfully applied this approach to the

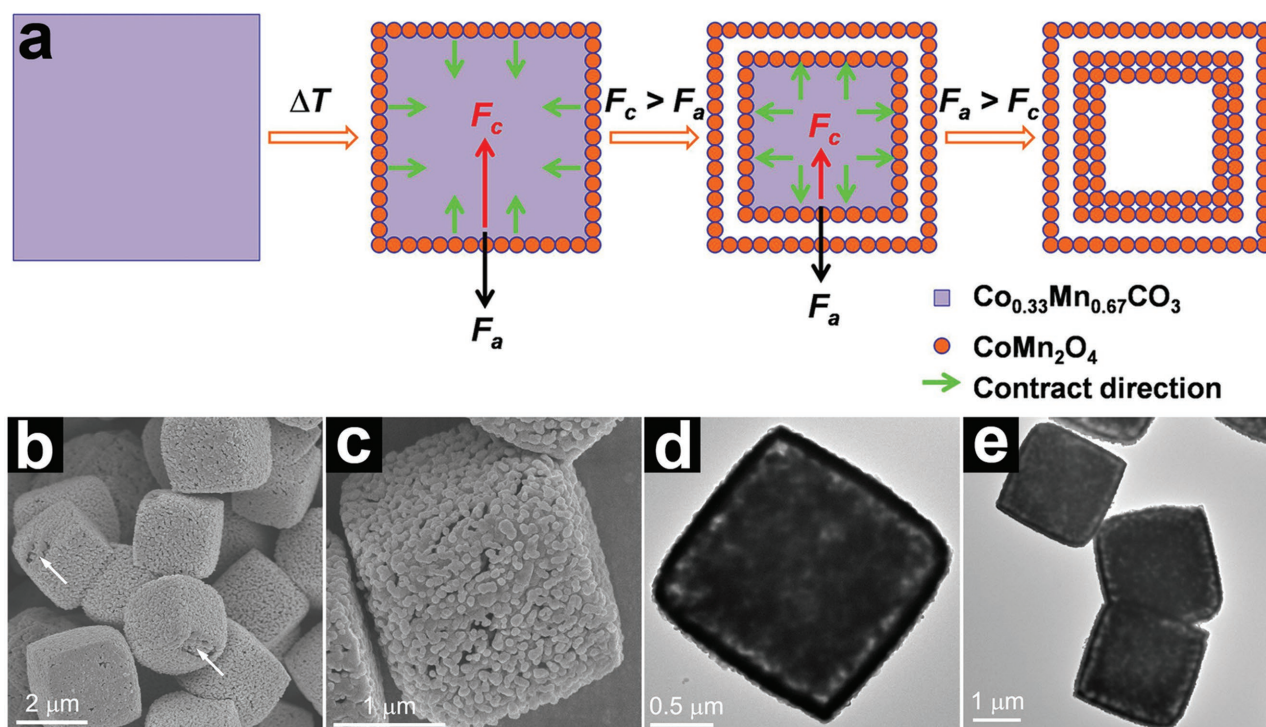


Figure 11. a) Schematic illustration for the fabrication of double-shelled CoMn_2O_4 hollow microcubes through thermal decomposition of $\text{Co}_{0.33}\text{Mn}_{0.67}\text{CO}_3$ microcubes. b–e) SEM (b,c) and TEM (d,e) images of double-shelled CoMn_2O_4 hollow microcubes. Reproduced with permission.^[76]

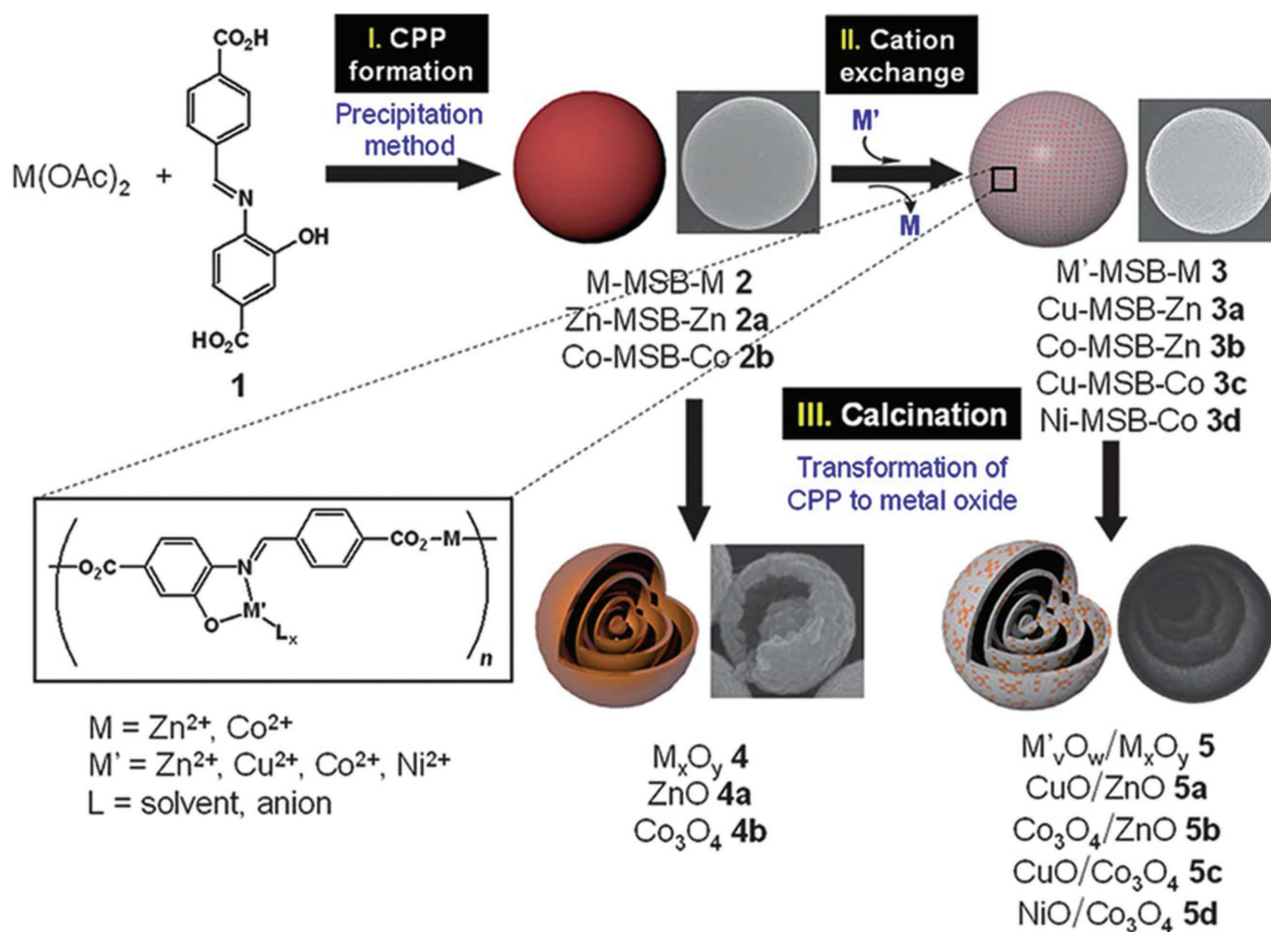


Figure 12. Schematic illustration for the preparation of metal oxide (ZnO and Co_3O_4) and hybrid metal oxide (CuO/ZnO, Co_3O_4/ZnO , CuO/ Co_3O_4 , and NiO/ Co_3O_4) multishell hollow spheres by thermal decomposition of coordination polymer particles (CPP). Reproduced with permission.^[77]

fabrication of multishelled CuO@NiO hollow spheres through heterogeneous thermal decomposition of Cu–Ni bimetallic organic frameworks.^[88] Zheng and co-workers prepared Co_3O_4 ball-in-dodecahedron hollow structures via annealing zeolitic imidazolate framework-67 (ZIF-67, $Co(2\text{-methylimidazole})_2$) in air.^[89]

Despite the success in fabricating metal oxide MSHSs via thermally decomposing MOFs, simply annealing MOFs in air usually leads to single-shelled hollow structures rather than their multishelled counterparts.^[90,91] To increase the structural complexity of the products, Lou and co-workers developed some novel strategies to convert MOFs into yolk-shell particles.^[92,93] With subsequent thermal decomposition in air or in an inert atmosphere, MSHSs can be formed. As the first example,^[92] they converted the surface of ZIF-67 into Ni–Co layered double hydroxide (Ni–Co LDH) by dispersing ZIF-67 in a $Ni(NO_3)_2$ ethanol solution. Upon calcination of the as-obtained ZIF-67@Ni–Co LDH yolk-shell structures in air, $Co_3O_4@NiCo_2O_4$ double-shelled nanocages (DSNCs) are produced. The inner Co_3O_4 shell is obtained from the thermal decomposition of the ZIF-67 core, while the outer $NiCo_2O_4$ shell is derived from the Ni–Co LDH. As the second example,^[93] the ZIF-67 rhombic dodecahedrons are converted into ZIF-67@amorphous CoS yolk-shell structures by a

solution sulfidation process. With subsequent annealing in N_2 , the ZIF-67 core is converted into Co-embedded carbon (Co–C), while the amorphous CoS shell is converted into Co_9S_8 . As a result, Co–C@ Co_9S_8 DSNCs are obtained. An intriguing feature of these DSNCs is that the inner and outer shells vary in composition. This unique feature endows the different shells with different functions, making the DSNCs multifunctional.

2.6.3. Thermal Decomposition of Metal Glycolate and Glycerate Spheres

Similar to MOFs, metal glycolates and glycerates also possess an organic moiety and inorganic metallic moiety. As a result, their thermal-decomposition behavior is quite similar to that of MOFs, and it is possible to form metal oxide MSHSs after thermal decomposition in air. Zhang et al. reported the synthesis of $ZnMn_2O_4$ DSHSs by a facile two-step method, which involves the solution synthesis of ZnMn-glycolate hollow microspheres and subsequent thermal decomposition in air.^[78] The competition between the contraction and adhesion forces drives the matter relocation and thus the shell separation. By using MnCo-glycolate spheres as the precursor, Xiong and co-workers extended this method to the preparation of a series of

MnCo₂O₄ hollow spheres with multilevel interiors, including mesoporous spheres, SSHSs, yolk-shell spheres, DSHSs, and core-in-double-shell hollow spheres.^[94] The structure modulation is achieved by tuning the temperature-ramping rate during thermal decomposition, which affects the balance between the contraction and adhesion forces. This concept is not limited to metal glycolates. Starting from NiCo-glycerate solid spheres, highly uniform NiCo₂O₄ core-in-double-shell hollow spheres can be obtained after thermal decomposition.^[79]

2.6.4. Thermal Decomposition of Metallic Species containing Carbonaceous Spheres

Carbonaceous spheres have long been employed as hard templates for the synthesis of hollow spheres.^[95–97] The carbonaceous polysaccharide spheres are usually prepared from glucose under hydrothermal conditions; the resultant carbonaceous colloids are hydrophilic in nature and rich in –OH and C=O functional groups.^[98] In the pioneering studies,^[95–97] the carbonaceous spheres were usually dispersed in low-concentration metal-salt solutions (0.05–0.5 M), and the metal ions mainly bind to the functional groups on the surface through coordination or electrostatic interactions. After calcination to remove the carbon, SSHSs are obtained as expected. The above process can be considered as true hard templating as the obtained SSHSs are negative replicas of the carbonaceous colloids.

Interestingly, quite different results can be obtained when the carbonaceous polysaccharide spheres are immersed in high-concentration metal-salt solutions.^[80,99] With a high concentration of metal salts, the metal ions not only absorb on the surface but also penetrate into the interior of carbonaceous spheres. The higher the concentration of metal salts is, the more the metal ions penetrate into the carbonaceous spheres.^[99] When heated

in air, the temperature gradient along the radial direction causes the first decomposition of the exterior surface and the formation of a rigid metal oxide shell. Further heating leads to the separation of the rigid metal oxide shell and inner core. The shell formation–separation process can be repeated several times, and multishelled metal oxide hollow spheres can be generated eventually.^[80] For example, multishelled α -Fe₂O₃ hollow structures can be prepared by metal-ion adsorption in high-concentration iron nitrate solution (2.0–5.0 M) followed by calcination in air.^[80] The number of shells can be well controlled by altering the concentration of metal salts; single-, double-, triple-, and quadruple-shelled α -Fe₂O₃ hollow spheres can be obtained at iron nitrate concentrations of 0.5, 2.0, 3.0, and 5.0 M, respectively.^[80] This approach can be generally applied to the preparation of various metal oxide multishelled hollow spheres, including α -Fe₂O₃,^[80,100] NiO,^[80] CuO,^[80] ZnO,^[101–104] Co₃O₄,^[105] SnO₂,^[106] TiO₂,^[107] Mn₂O₃,^[108,109] WO₃,^[110] V₂O₅,^[111] and MFe₂O₄ (M = Zn, Co, Ni, Cd).^[99] Besides the concentration of the metal-salt solution, the solvent type,^[100,105] heating rate,^[101] pH value,^[105,108] and immersion period^[107] also play significant roles in manipulating the structural parameters of the metal oxide hollow structures, such as the number of shells, the shell thickness, and the intershell spacings (Figure 13a). For example, immersion of the carbonaceous spheres in 1.0 M [Co(H₂O)₆]²⁺ aqueous solution followed by calcination in air results in single-shelled Co₃O₄ hollow spheres (Figure 13b).^[105] Replacing half of the water with ethanol (ethanol:water = 1:1, v/v) decreases the number of coordinated water molecules and improves the penetration capability of hydrated cobalt ions [Co(H₂O)_{6-x}]²⁺, producing double-shelled Co₃O₄ hollow spheres (Figure 13c). Further increasing the fraction of ethanol and increasing the temperature of the solution generate triple-shelled Co₃O₄ hollow spheres (Figure 13d). Treating the carbonaceous spheres with HCl results in quadruple-shelled Co₃O₄ hollow spheres (Figure 13e).

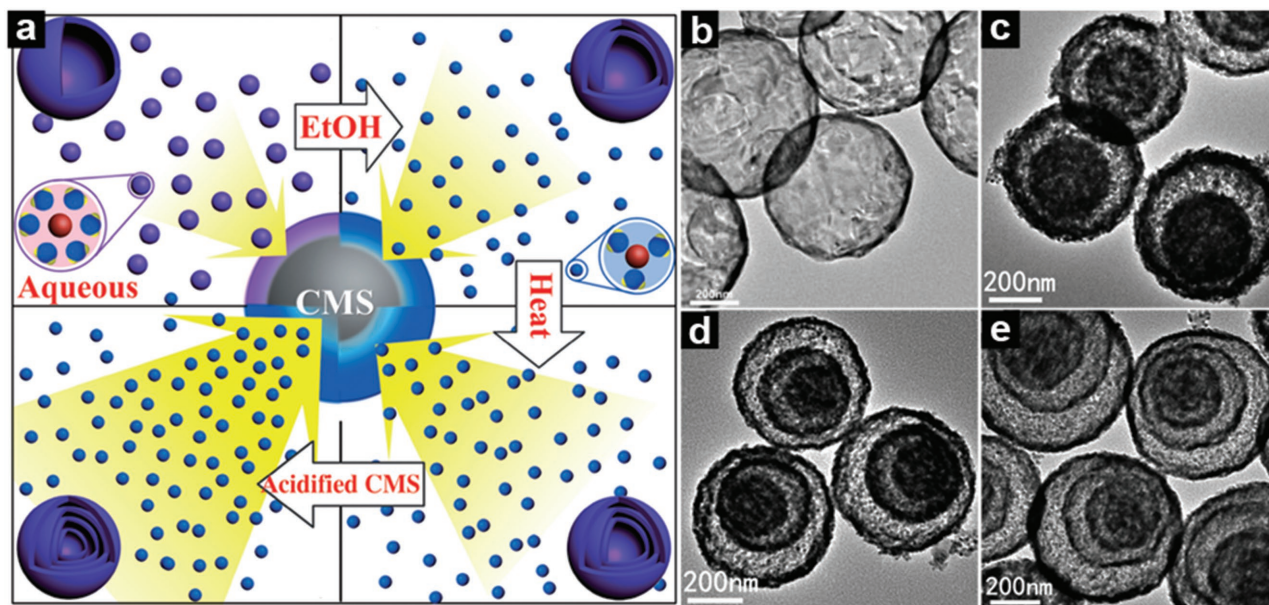


Figure 13. a) Schematic illustration for the formation of multishelled Co₃O₄ hollow spheres under different conditions. b–e) TEM images of single-shelled (b), double-shelled (c), triple-shelled (d), and quadruple-shelled (e) Co₃O₄ hollow spheres. Reproduced with permission.^[105]

Dispersion of carbonaceous spheres in low-concentration metal-salt solution can also result in multishelled hollow spheres if precipitants (such as urea) are introduced in the solution. For example, Xu and co-workers reported the synthesis of various metal oxide hollow spheres with uniform size by controlled precipitation of metal cations on carbonaceous spheres followed by calcination.^[112] Although low-concentration ferric chloride and nickel nitrate are used in the synthesis, the Fe_2O_3 and NiO obtained exhibit a double-shelled hollow spherical structure. This route is dependent on the controlled precipitation induced by the hydroxyl anions slowly released from the decomposition of urea. Cao and co-workers reported the fabrication of carbonaceous sphere@ $\text{Co}_2\text{CO}_3(\text{OH})_2$ core-shell composites via a similar controlled precipitation approach and multishelled Co_3O_4 hollow spheres can be obtained after subsequent calcination.^[113] By repeating the controlled precipitation process, Zhang and co-workers reported the fabrication of single-, double-, and triple-shelled NiO hollow spheres.^[114]

Recently, Zhang and Lou developed a general “penetration–solidification–annealing” strategy for the fabrication of multishelled ternary metal oxide hollow spheres, including CoMn_2O_4 , $\text{Co}_{1.5}\text{Mn}_{1.5}\text{O}_4$, MnCo_2O_4 , ZnMn_2O_4 , ZnCo_2O_4 , and NiCo_2O_4 .^[115] In this approach, the carbonaceous polysaccharide spheres are first dispersed in an ethylene glycol solution of metal acetate precursors. To realize the deep “penetration” of metal ions into the carbonaceous spheres, the reaction solution is heated up to 120 °C with stirring for 12 h. The refluxing of the dispersion at 170 °C for 2 h generates metal glycolate–carbonaceous composite spheres (“solidification”). With subsequent thermal annealing in air, multishelled hollow spheres are obtained. With a similar strategy, Hu and co-workers successfully prepared multishelled $\alpha\text{-Fe}_2\text{O}_3$ hollow spheres.^[116]

Although effective, the above-mentioned strategies for fabricating single- and multishelled hollow spheres from carbonaceous spheres require multiple steps. In general, these processes involve the preparation of carbonaceous colloids via a hydrothermal treatment, isolation and purification of the carbonaceous colloids, metal-ion adsorption, penetration, or precipitation, and finally carbon removal via calcination. To simplify the synthetic process, Thomas and co-workers directly prepared metal-ion-incorporated carbonaceous spheres via a simple one-pot hydrothermal treatment, during which the “polymerization” of carbohydrate and adsorption of metal ions occur simultaneously.^[117] Upon calcination in air, various metal oxide hollow spheres, such as Fe_2O_3 , NiO, Co_3O_4 , CeO_2 , MgO, and CuO, can be obtained. However, these hollow spheres are generally single-shelled. Yang, Cao, and co-workers applied this strategy to synthesize multishelled SnO_2 hollow spheres by hydrothermally treating $\text{SnCl}_4 \cdot 5\text{H}_2\text{O}$ and sucrose followed by calcination.^[118] Wu, Lu, and Wang further extended this approach to the preparation of double-shelled TiO_2 hollow spheres.^[119] Based on a similar approach, MFe_2O_4 (M = Co, Ni, Cd),^[120] Cr_2O_3 ,^[121] ZnO ^[122] and $\text{La}_{0.9}\text{Sr}_{0.1}\text{CoO}_3$ ^[123] multishelled hollow spheres have also been prepared. Tang and co-workers constructed multishelled CeO_2 hollow spheres via hydrothermally treating cerium chloride, urea, and glucose with subsequent annealing.^[124] Zou and co-workers reported a family of multishelled hollow spheres via hydrothermal treating metal gluconate followed by heating in air.^[125] These metal oxides include,

but are not limited to Co_3O_4 , CuO, Fe_2O_3 , In_2O_3 , $\text{PrO}_{1.83}$, and ZnO.

It should be pointed out that the preparation of multishelled hollow spheres from metallic species containing carbonaceous spheres are usually categorized as hard-templating method in the literature.^[9,16,19] However, the as-obtained multishelled hollow spheres are not truly negative replicas of the “templates”. Instead, the non-equilibrium heat-treatment-induced heterogeneous contraction plays a significant role in the formation of multishelled hollow spheres. Considering the above-mentioned facts, herein, we classify this process as thermally induced matter relocation rather than hard templating.

2.6.5. Spray-Drying-Assisted Synthesis

Despite the rapid developments of synthetic technologies in the last few decades, the versatile, economic, and mass production of MSHSs remains a great challenge. Spray-drying is a widely employed technique in chemical, pharmaceutical, and food industries for producing dry powders from a solution, dispersion or slurry depending on droplet-to-particle processes.^[126,127] It provides a unique opportunity for the rapid, continuous, cost-effective, reproducible, and scalable production of fine particles, especially those with spherical shape. The spray-drying process generally consists of three fundamental steps: i) atomization of the fluid into fine droplets, ii) solvent evaporation and formation of dry particles, and iii) separation and collection of dry particles from the drying gas. Depending on the operating conditions, either solid or hollow particles can be produced.^[128]

Although the preparation of hollow spheres by spray drying has been demonstrated for a long time, the synthesis of multishelled hollow spheres was not realized until recently. Recently, Zhou et al. developed a facile method for the low-cost and scalable production of $\alpha\text{-Fe}_2\text{O}_3$ multishelled hollow spheres by simply spray-drying an aqueous solution of iron nitrate and sucrose with subsequent annealing in air (Figure 14a–c).^[82] The spray-drying process produces iron nitrate–sucrose composite microspheres, in which the iron nitrate is uniformly distributed in the sucrose matrix. With subsequent annealing in air, the sucrose is burnt off and the iron nitrate is decomposed into $\alpha\text{-Fe}_2\text{O}_3$. Due to the non-equilibrium heat-treatment-induced heterogeneous contraction, $\alpha\text{-Fe}_2\text{O}_3$ multishelled hollow spheres are obtained (Figure 14d). In agreement with the non-equilibrium heat-treatment-induced heterogeneous contraction mechanism, the number of shells can be generally controlled by the temperature-ramping rate during annealing in air; a high ramping rate leads to more shells, while a low ramping rate results in fewer shells. More importantly, this method (“spray-drying-then-annealing”) is quite versatile. The sucrose matrix can be replaced with other organic species such as glucose, oxalic acid, citric acid, poly(vinyl alcohol) (PVA), PVP, and poly(ethylene glycol) (PEG), while the iron nitrate can be substituted with other metal salts as well.^[129] As a result, a wide variety of TMO multishelled hollow spheres, such as $\alpha\text{-Fe}_2\text{O}_3$, Cr_2O_3 , V_2O_5 , ZnFe_2O_4 , and iron-titanium oxide (Fe–Ti–O), can be produced with this novel method.^[129]

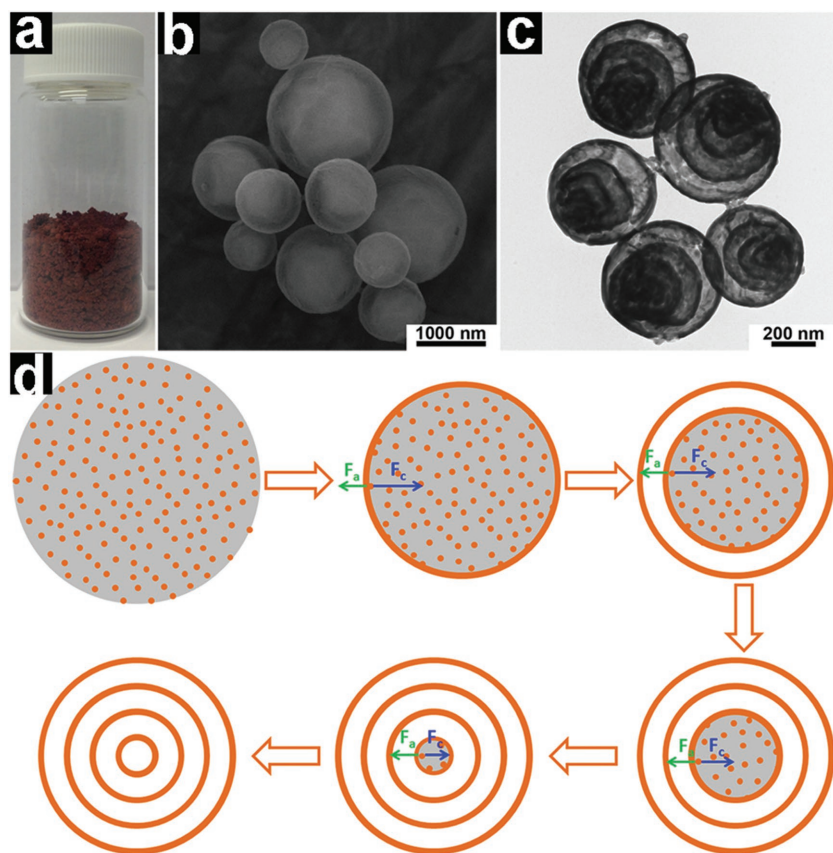


Figure 14. a–d) Digital photograph (a), SEM image (b), TEM image (c), and schematic formation mechanism (d) of α - Fe_2O_3 multishelled hollow spheres. Reproduced with permission.^[82] Copyright 2013, Royal Society of Chemistry.

Although α - Fe_2O_3 multishelled hollow spheres can be easily produced via spray-drying of iron nitrate and sucrose followed by annealing in air, some problems associated with the utilization of iron nitrate still exist. First, iron nitrate is a strong oxidant, the spray-drying of which may cause unacceptable safety hazards. Second, iron nitrate is highly hygroscopic. Due to its hygroscopicity, well-defined α - Fe_2O_3 multishelled hollow spheres can only be obtained in a relatively narrow sucrose/iron nitrate range (from 0.75 to 1.0). Third, the decomposition of iron nitrate generates highly toxic gases such as NO_x . To overcome these problems, Padashbarmchi et al. screened a variety of iron-containing precursors and found that iron (III) citrate is an ideal precursor to replace iron nitrate in spray-drying.^[130] This modification in precursor, although it seems simple, can effectively eliminate the above-mentioned problems, making the mass production of α - Fe_2O_3 multishelled hollow spheres more viable.

The hygroscopicity of metal precursors and the caramelization of organic species during the spray-drying process represent two detrimental factors for spray-drying. Both issues can be circumvented by the judicious selection of metal-salt precursors and organic matrixes.^[82,130] Based on the “spray-drying-then-annealing” strategy, Choi and Kang reported the mass production of SnO_2 yolk-shell structures using dextrin as the organic matrix and tin oxalate as

the metal precursor.^[131] The utilization of dextrin as the organic matrix enables the production of dry precursor particles (tin oxalate–dextrin composite microspheres) with low hygroscopicity under high humidity. By a similar approach, ZnFe_2O_4 multishelled hollow spheres have been fabricated by the same group through spray-drying zinc nitrate, iron nitrate, and dextrin with subsequent annealing in air.^[132] By applying a gas-phase sulfidation process to the ZnFe_2O_4 multishelled hollow spheres, Zn–Fe–S multishell hollow spheres consisting of sphalerite $\text{Zn}_x\text{Fe}_{1-x}\text{S}$ solid solution and hexagonal FeS can be obtained.^[133] Lee, Kang, and co-workers prepared multishelled Co_3O_4 hollow spheres with 4–6 shells by spray-drying an aqueous solution of cobalt nitrate, citric acid, and ethylene glycol followed by calcination in air.^[134] The esterification reaction between the citric acid and the ethylene glycol during the spray-drying plays a significant role in producing dense, spherical, and non-aggregated precursor particles with low hygroscopicity, which is essential for the subsequent formation of well-defined multishelled Co_3O_4 hollow spheres. With the introduction of palladium nitrate into the precursor solution, Pd-loaded quintuple-shelled Co_3O_4 hollow spheres can be successfully obtained.^[135]

Although suitable for mass production, the spray-drying process usually generates polydisperse spherical particles. The preparation of monodisperse hollow spheres by spray drying remains a great challenge. Recently, Selomulya, Zhao, and co-workers reported the fabrication of monodisperse, ordered mesoporous-carbon hollow microspheres with a size of approximately $61.0\ \mu\text{m}$ by a unique microfluidic jet-spray-drying technology.^[136] It can be expected that large, monodisperse multishelled hollow spheres may be obtained by coupling the microfluidic jet spray drying and thermally induced mass relocation.

2.6.6. Spray Pyrolysis

Spray pyrolysis is a technology similar to spray-drying. Despite their great similarity in operating principles, substantial differences still exist. First, the operating temperature of the spray-pyrolysis process ($>600\ ^\circ\text{C}$) is significantly higher than that of spray-drying ($<300\ ^\circ\text{C}$).^[131] Due to the high operating temperature, an additional thermal-decomposition process may occur after drying of the droplets in spray pyrolysis. Second, the production efficiency of the spray-pyrolysis process is tens of times lower than that of similar-scale spray-drying.^[135]

In 2007, Sun and co-workers prepared hollow spherical NiO with a yolk-shell structure by ultrasonic spray pyrolysis.^[137] However, this specific structure did not attract much attention at

that time. Recently, Kang and co-workers reported the synthesis of yolk-in-double-shell-structured SnO_2 by the spray-pyrolysis method using tin oxalate and sucrose as precursors.^[138] This facile and powerful strategy was soon extended to the fabrication of other binary oxides (such as Co_3O_4 , Fe_2O_3 , V_2O_5 , WO_3 , NiO , and MoO_3),^[139–144] ternary oxides (such as LiMn_2O_4 , CoMn_2O_4 , ZnCo_2O_4 , LiV_3O_8 , $\text{Li}_4\text{Ti}_5\text{O}_{12}$, and NiCo_2O_4),^[145–150] quaternary oxides ($\text{LiNi}_{0.5}\text{Mn}_{1.5}\text{O}_4$),^[151] metal-oxide–metal-oxide composites (such as $\text{CuO–Fe}_2\text{O}_3$, $\text{In}_2\text{O}_3\text{–NiO}$, Zn–Mn–O , Ti–Al–Zr–Ce–Y–O , $\text{Co–Cu–Fe–Mn–Mo–Ni–Zn–Cr–W–V–O}$),^[152–156] and noble-metal–metal-oxide composites (Pd–SnO_2),^[157] with yolk-shell, yolk-in-multishell, or multishelled hollow structures. The number of shells can be easily manipulated by adjusting the synthetic parameters such as the pyrolysis temperature.^[140,150] In addition, the obtained metal oxide multishelled hollow spheres can be effectively converted into the corresponding metal sulfide with a similar structure by employing a sulfidation process. As a proof-of-concept, SnS ,^[158] Co_9S_8 ,^[159] MoS_2 ,^[160] and SnS–MoS_2 ^[161] multishelled hollow spheres have been prepared.

Table 1 summarizes some typical MSHSs, including their composition, geometry, and synthetic method. It should be pointed out that, with the rapid development of nanotechnology, some novel synthetic approaches have been developed to prepare specific MSHSs, while these approaches are not included in the above-mentioned six categories. For example, Lou and co-workers developed a template-engaged redox etching approach to prepare double-walled $\text{Fe}(\text{OH})_x$ hollow cages;^[162] González et al. designed polymetallic hollow nanoparticles with high complexity, such as double-walled nanocages, by sequential galvanic exchange and Kirkendall growth.^[75]

3. Synthetic Strategies for Beyond Multishelled Hollow Structures

As mentioned in Section 2, the MSHS can be considered to be an assembly of single-shelled hollow structures in a concentric or eccentric way. Besides MSHSs, there are a wide variety of intricate hollow structures. For example, SSHSs can further assemble into secondary spheres, hollow spheres, and fibers, forming bubble-within-bubble, bubble-within-sphere, and bubble-within-fiber structures, respectively. Apart from SSHSs, yolk-shell spheres and nanotubes can also be used as the building blocks for constructing higher level hollow structures, such as pomegranate-like structure. The bubble-within-bubble, bubble-within-sphere and pomegranate-like structures possess the advantages of not only hollow/yolk-shell nanospheres, but also micrometer-sized assemblies. As a result, these intricate hollow structures are more advantageous than the primary hollow and yolk-shell nanospheres in energy storage and conversion applications. These novel intricate hollow structures will be reviewed in this section.

3.1. Bubble-Within-Bubble and Bubble-Within-Sphere Structures

Yec and Zeng reported a surface-catalyzed dual-templating process for the synthesis of manganese silicate

nanobubble-constructed hollow microspheres, the so-called bubble-within-bubble structure (**Figure 15a–c**).^[167] The primary nanobubbles have a size of 7–9 nm, while the secondary hollow spheres have a much larger size of ≈ 270 nm. The synthesis of the manganese silicate bubble-within-bubble structure involves the hydrothermal treatment of Stöber SiO_2 spheres in the presence of manganese acetate. It is proposed that the Mn(II) serves as the catalysts for the decomposition of carboxylate anions; the gases generated in situ (such as CO_2) from the decomposition of carboxylate anions act as the soft template directing the formation of the manganese silicate nanobubbles; meanwhile, the Stöber SiO_2 beads function as the hard template directing the assembly of the tiny nanobubbles into hollow microbubbles.^[167] A wide variety of foreign metal ions (such as Fe, Co, Ni, Cu, Y, La, Ce, Nd, Eu, Gd, Er, and Yb) can be introduced into the manganese silicate by mixing foreign metal salts with the manganese acetate during the hydrothermal synthesis.^[167] In order to pursue multifunctionality or a synergistic effect between the different components, various functional cores including metal nanoparticles (Au, Ag, Pt, Ni, Co, and Au–Pd alloy), metal oxide nanoparticles (MoO_2 and Fe_3O_4), carbon nanotubes (CNTs), and their combinations can be encapsulated into the hollow cavities of the secondary particles.^[168]

Cho et al. reported the fabrication of Fe_2O_3 microspheres composed of hollow nanospheres (**Figure 15d–f**), the so-called bubble-within-sphere structure, by a three-step process.^[169] In the first step, FeO_x –carbon composite microspheres are prepared by directly spray pyrolysis of a precursor solution containing iron nitrate and sucrose. The FeO_x –carbon microspheres are then reduced to Fe–carbon by annealing in H_2/Ar at 500 °C. Lastly, the Fe–carbon composite spheres are transformed into bubble-within-sphere-structured Fe_2O_3 by reoxidation, during which nanoscale Kirkendall diffusion plays a vital role. Using a similar approach, NiO hollow microspheres constructed from hollow nanospheres (bubble-within-bubble structure) are fabricated starting from nickel nitrate and PVP.^[170]

3.2. Bubble-Within-Fiber Structure

Cho et al. reported the fabrication of bubble-within-fiber-structured Fe_2O_3 –C composite nanofibers (**Figure 16a**), which were composed of Fe_2O_3 nanobubbles uniformly distributed in an amorphous carbon-fiber matrix, by combining the Kirkendall effect with the electrospinning method.^[171] The synthesis process involves three main steps: i) the synthesis of iron acetylacetonate–polyacrylonitrile ($\text{Fe}(\text{acac})_3$ –PAN) composite fibers by electrospinning; ii) the reduction of Fe(III) to metallic Fe nanocrystals and the carbonization of organic species; and iii) the reoxidation of metallic Fe nanocrystals to Fe_2O_3 under air. Due to the fast outward diffusion of Fe^{3+} and slow inward diffusion of O^{2-} during annealing in air (the Kirkendall effect), the metallic Fe nanocrystals are transformed into Fe_2O_3 nanobubbles. This simple synthetic strategy can be generally applied to the fabrication of bubble-within-fiber-structured metal oxide nanofibers and metal-oxide–carbon composite nanofibers. For example, bubble-within-bubble-structured nanofibers composed of Sn@void@SnO/SnO_2 yolk-shell

Table 1. Summary of typical multishell hollow structures.

Year	Composition	Structure	Methodology	Refs.
1998	SiO ₂	Vesicles	Soft templating	[44]
2005	TiO ₂ , Fe ₃ O ₄ , polyaniline	DSHSs	Hard templating	[37,38]
2007	SnO ₂	Double-shelled hollow structures	Hard templating	[34,36]
2007	Fe ₂ O ₃ , NiO	DSHSs	Thermally induced matter relocation	[112]
2007	Cu ₂ O	MSHSs	Soft-templating	[49]
2007	SnO ₂	MSHSs	Thermally induced matter relocation	[118]
2007	Cu ₂ O	MSHSs	Intermediate-templating assembly	[163]
2008	Organosilica	Vesicles	Soft templating	[46]
2009	V ₂ O ₅	DSHSs	Ostwald ripening	[164]
2010	C	Vesicles	Soft templating	[47]
2010	Fe ₂ O ₃	MSHSs	Thermally induced matter relocation	[81]
2010	PMMA, SiO ₂	DSHSs, core-in-double-shell hollow spheres	Hard templating	[28]
2010	Co ₃ O ₄	MSHSs	Soft templating	[51]
2010	Fe(OH) _x	Double-walled hollow cages	Template-engaged redox etching	[162]
2010	TiO ₂	MSHSs	Thermally induced matter relocation	[22]
2011	ZnO, Co ₃ O ₄	MSHSs	Thermally induced matter relocation	[77]
2011	Metals	Double-walled hollow cages	Sequential galvanic exchange and Kirken-dall growth	[75]
2011–2016	Fe ₂ O ₃ , ZnO, Co ₃ O ₄ , SnO ₂ , TiO ₂ , Mn ₂ O ₃ , WO ₃ , V ₂ O ₅	MSHSs	Thermally induced matter relocation	[80,100,101,105–108,110,111]
2011	SiO ₂	MSHSs	Selective etching of “soft@hard” particles	[58]
2011	TiO ₂	DSHSs	Thermally induced mass relocation	[119]
2011	Cu ₂ O	MSHSs	Ostwald ripening	[70]
2012	Cu ₂ S	MSHSs	Ion exchange	[72]
2012	Cu ₂ O	MSHSs	Ostwald ripening	[71]
2012	CoMn ₂ O ₄	Double-shelled hollow cubes	Thermally induced mass relocation	[76]
2012–2015	MMn ₂ O ₄ , MCo ₂ O ₄ , Co _{1.5} Mn _{1.5} O ₄	MSHSs	Thermally induced mass relocation	[78,79,94,115]
2012	C	DSHSs	Hard templating	[39]
2013	SnO ₂	MSHSs	Thermally induced mass relocation	[138]
2013	PB	Double-shelled hollow cages	Selective etching of “soft@hard” particles	[67]
2013	Co ₃ O ₄ , CuO, Fe ₂ O ₃ , In ₂ O ₃ , PrO _{1.83} , ZnO	MSHSs	Thermally induced mass relocation	[125]
2013	CoSn(OH) ₆	Multishelled hollow cages	Selective etching of “soft@hard” particles	[63]
2013	Fe(OH) ₃	Multishelled hollow boxes	Template engaged reactions	[87]
2013	Fe ₂ O ₃	MSHSs	Thermally induced mass relocation	[82]
2014	MS	Box-in-box hollow structures	Template-engaged method	[165]
2014–2015	Co ₃ O ₄ , CuO@NiO	Multishelled hollow structures	Thermally induced mass relocation	[88,89]
2015–2016	Co ₃ O ₄ @NiCo ₂ O ₄ , Co–C@Co ₉ S ₈ , Co(OH) ₂ @LDH	Double-shelled hollow cages	Thermally induced mass relocation	[92,93,166]
2015	TiO ₂ , TiO ₂ /SiO ₂	MSHSs	Hard templating	[25–27]
2015	NiCo ₂ S ₄	DSHSs	Ion exchange	[73]
2015	PMO	MSHSs	Selective etching of “soft@hard” particles	[59]
2015	C	MSHSs	Hard templating	[32]

nanospheres,^[172] hollow SnO/SnO₂ nanospheres,^[172] hollow SnO₂ nanospheres,^[172] hollow NiO nanospheres,^[173] and hollow CoFe₂O₄@onion-like graphitic carbon nanospheres^[174] have been prepared by using a similar approach.

3.3. Pomegranate-Like Structure

Cui and co-workers developed a bottom-up microemulsion approach for the fabrication of silicon-based pomegranate-like

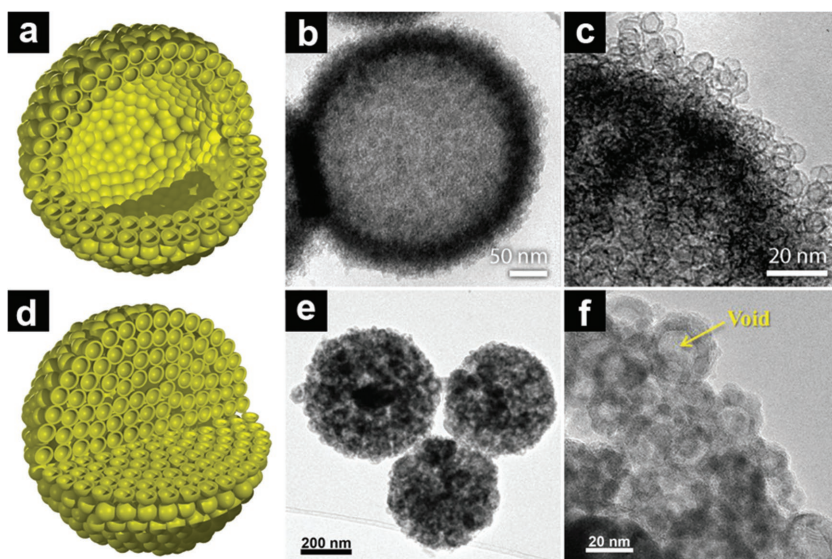


Figure 15. a) Schematic illustration of the bubble-within-bubble structure. b, c) TEM images of the bubble-within-bubble structured manganese silicate. a–c) Reproduced with permission.^[167] Copyright 2014, American Chemical Society. d) Schematic illustration of the bubble-within-sphere structure. e, f) TEM images of the bubble-within-sphere structured Fe₂O₃. Reproduced with permission.^[169] Copyright 2015, Royal Society of Chemistry.

microspheres with sizes of 0.5–10 μm (Figure 16b).^[175] The micrometer-sized secondary spheres are composed of sub-micrometer-sized Si@void@carbon primary nanoparticles. Each individual silicon nanoparticle is well encapsulated by a carbon shell with a void in between. The synthesis of such a unique pomegranate-like structure involves four fundamental steps: i) synthesis of Si@SiO₂ primary particles using the Stöber method; ii) assembly of the Si@SiO₂ nanoparticles into microspheres using a microemulsion approach; iii) carbon coating, and iv) SiO₂ sacrificial layer etching. To avoid the utilization of highly toxic hydrofluoric acid (HF), an alternative approach has been developed by Dou, Liu and co-workers to

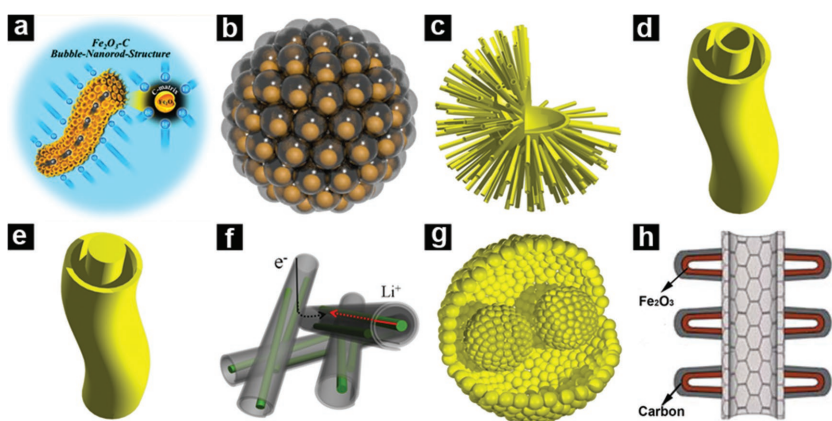


Figure 16. a–h) Schematic illustrations of bubble-within-fiber structured Fe₂O₃-C (a), pomegranate-like microspheres (b), nanotube-constructed hollow spheres (c), tube-in-tube structure (d), wire-in-tube structure (e), semihollow scroll (f), double-yolk egg structure (g), and carbon-coated α-Fe₂O₃ hollow nanohorns on CNT (h). a) Reproduced with permission.^[171] Copyright 2015, American Chemical Society. b) Reproduced with permission.^[175] Copyright 2014, Nature Publishing Group. f) Reproduced with permission.^[176] Copyright 2013, American Chemical Society. h) Reproduced with permission.^[177] Copyright 2012, Royal Society of Chemistry.

prepare silicon-based microspheres with a similar pomegranate-like structure.^[178] In this approach, the silicon nanoparticles are first encapsulated in CaCO₃ by a co-precipitation reaction to obtain Si@CaCO₃ microspheres. The CaCO₃ is then decomposed into CaO under thermal treatment and coated with a carbon shell by a chemical vapor deposition (CVD) process. Finally, the CaO is etched off with dilute HCl, leaving behind Si@void@C pomegranate-like microspheres.

3.4. Nanotube-Constructed Hollow Spheres

The above-mentioned bubble-within-bubble, bubble-within-sphere, bubble-within-fiber, and pomegranate-like structures are built up with 0D hollow or yolk-shell nanospheres. The 1D nanotubes can be used as the building blocks to construct hollow structures with higher complexity as well. Wang et al. have reported the fabrication of copper silicate hollow spheres constructed from nanotubes (Figure 16c) via a simple

one-pot hydrothermal method by using Stöber SiO₂ spheres as the templates.^[179] The primary nanotubes are ultrafine in diameter; their average outer and inner diameters are around 8 and 3.5 nm, respectively. The scrolling of layer-structured copper silicate at an elevated temperature and pressure are responsible for the formation of the primary nanotubes. Sheng and Zeng developed a general complex-assisted ion-exchange method to dope the copper silicate nanotube-constructed hollow spheres with various 3d transition metals (M = Mn, Fe, Co, Ni, and Zn).^[180] Up to 80% of the Cu²⁺ in the octahedral sites of copper silicate can be replaced with dopant metal ions with the original nanotube structure unaffected. Zhang et al. extended this method to the fabrication of other transition metal silicate (such as cobalt silicate and manganese silicate) hollow spheres constructed from 1D nanotube building blocks.^[181] Tang, Mai, and co-workers introduced graphene oxide during the hydrothermal synthesis of copper silicate hollow spheres and obtained a copper-silicate-hollow-sphere-reduced-graphene-oxide composite.^[182] The introduction of graphene oxide affects neither the overall hollow spherical morphology nor the primary tubular structure of the copper silicate.

3.5. Tube-in-Tube and Wire-in-Tube Structures

The 1D tube-in-tube and wire-in-tube structures can be regarded as analogs of the 0D MSHS and yolk-shell structures, respectively.^[3] Such 1D tube-in-tube and wire-in-tube structures have efficient charge-transfer pathways, which is essential for

energy storage and conversion applications. Although diverse 0D MSHSs and yolk-shell structures have been reported, reports on 1D tube-in-tube and wire-in-tube structures are relatively rare. Despite this fact, some 1D tube-in-tube and wire-in-tube nanostructures have successfully been created by ingenious strategies.

Guan and co-workers demonstrated the fabrication of maghemite ($\gamma\text{-Fe}_2\text{O}_3$) tube-in-tube (Figure 16d) and wire-in-tube (Figure 16e) nanostructures based on single-spinneret electrospinning and non-equilibrium heat treatment.^[183] Precursor fibers composed of PVP and iron citrate are prepared by an electrospinning technique. The electrospun gel fibers are then thermally treated. By adjusting the heating rate, the temperature gradient (ΔT) along the radial direction of the precursor fibers can be tuned, and thus the contract direction of the precursor fibers can be controlled. As a result, the structure of the final products can be tuned from solid nanofibers to hollow nanofibers, wire-in-tube nanostructures, and tube-in-tube nanostructures through adjusting the heating rate. This method can be generally applied to the fabrication of other metal oxide tube-in-tube and wire-in-tube 1D nanostructures.^[184–188] For example, Xu and co-workers extended this method to the fabrication of tube-in-tube-structured TiO_2 nanofibers using tetra-*n*-butyl titanate ($\text{Ti}(\text{OC}_4\text{H}_9)_4$) and PVP as the starting materials.^[184] The $\text{Ti}(\text{OC}_4\text{H}_9)_4$ concentration and pinhole diameter of the jet head play a significant role as to the morphology and structure of the final products. Solid, hollow, and tube-in-tube-structured TiO_2 nanofibers can be obtained at high, middle, and low concentrations of $\text{Ti}(\text{OC}_4\text{H}_9)_4$, respectively. ZrO_2 , SiO_2 , SnO_2 , and In_2O_3 tube-in-tube-structured nanofibers can also be constructed by simply changing the precursors.^[184]

Chen, Ramakrishna, and co-workers developed a modified electrospinning method for the fabrication of ternary TMO tube-in-tube nanostructures, including CoMn_2O_4 , NiCo_2O_4 , CoFe_2O_4 , NiMn_2O_4 , and ZnMn_2O_4 .^[185] In this approach, two types of polymers, PAN and PVP, are employed in electrospinning. Due to the strong interactions between the PVP and the metal ions as well as the incompatibility between the PVP and the PAN, the PAN, PVP, and metal precursor undergo phase separation during the electrospinning process. The resultant electrospun nanofibers possess a unique core-shell configuration with a PAN-rich core and PVP/metal-ion-rich shell. The subsequent non-equilibrium heat treatment leads to the formation of tube-in-tube nanofibers.

Lou, Xie, and co-workers developed an alternative method for the general synthesis of metal oxide tube-in-tube nanostructures, including ternary CuCo_2O_4 , ZnCo_2O_4 , CoMn_2O_4 , ZnMn_2O_4 , MnCo_2O_4 , and NiCo_2O_4 , and binary Mn_2O_3 , Co_3O_4 , NiO , and Fe_2O_3 .^[189] Carbon nanofibers (CNFs) with abundant functional groups on the surface are used as the templates. In the first step, a metal glycolate layer is coated on the CNF surface to form a CNF@metal glycolate core-shell structure through a facile polyol method. The functional groups on the CNF surface ensure the successful coating. In the second step, the CNF@metal glycolate hybrid structure is annealed in air. The non-equilibrium heat treatment induces the formation of the complex tube-in-tube structures.

3.6. Semihollow Scroll

Mai and co-workers demonstrated an “oriented assembly” and “self-scroll” mechanism for the construction of semihollow bicontinuous graphene scrolls using V_3O_7 and MnO_2 nanowires as the templates (Figure 16f).^[176] The rapid growth of template nanowires, the oriented assembly of graphene sheets on the surface of the template nanowires, and the self-scroll of graphene ribbons are responsible for the formation of such unique nanostructure. These nanowire-templated graphene scrolls with free space between the nanowire and scroll can provide continuous diffusion pathways for both electrons and ions.

3.7. Multi-Yolk Egg Structure

Multi-yolk egg structures are commonly observed in nature, e.g., volvox algae.^[190] Inspired by opening of soft drink cans, Wang et al. developed a bubble-mediated approach for the fabrication of ZnO hollow spheres with a double-yolk egg structure (Figure 16g). The ZnO double-yolk eggs are obtained by solvothermal reaction of zinc acetate dihydrate in ethanalamine with constant gas flow in and out of the autoclave. With a modified approach, ZnO hollow spheres with triple-yolk egg structure can also be obtained.^[191] When coupled with two ion-exchange steps (S^{2-} ion-exchange and Cd^{2+} ion-exchange), ZnO/CdS composite hollow spheres with triple-yolk egg structure can be obtained.

3.8. Hollow Nanohorns on CNT

Lou and co-workers reported a novel hierarchical nanostructure with carbon-coated $\alpha\text{-Fe}_2\text{O}_3$ hollow nanohorns grafted on CNT backbones (Figure 16h).^[177] $\beta\text{-FeOOH}$ nanospindles are first grafted onto hydrophilic CNTs by forced hydrolysis of FeCl_3 . The $\beta\text{-FeOOH}$ nanospindles are then converted into $\alpha\text{-Fe}_2\text{O}_3$ hollow nanohorns by thermal treatment. Lastly, an amorphous carbon layer is coated on the surface of the hierarchical CNT@ Fe_2O_3 by hydrothermal carbonization of glucose.

4. Applications in Energy Storage and Conversion

4.1. Lithium-Ion Batteries

LIBs are well-known energy-storage devices.^[192–194] A typical LIB is composed of three indispensable components: a cathode, an anode, and an ionically conductive electrolyte. During charge and discharge, the lithium ions shuttle between the cathode and anode. Owing to the high energy density, light weight, no memory effect, small self-discharge, and environmental friendliness, LIBs have monopolized the power supplies for portable electronics. They have also been recognized as the power source of choice for upcoming electric vehicles, hybrid electric vehicles, and plug-in hybrid electric vehicles. These newly emerging applications have placed ever-increasing demands on the energy density of LIBs, which cannot be met by the existing LIB technology based on a lithium metal

oxide (LiMO_2 and LiMn_2O_4)/lithium iron phosphate (LiFePO_4) cathode and a graphite/lithium titanium oxide ($\text{Li}_4\text{Ti}_5\text{O}_{12}$) anode. Further breakthroughs can be expected from the development of advanced new electrode materials and structures.

Hollow structures provide a great opportunity to boost the lithium-storage performance of electrode materials in terms of specific capacity, cycling stability, and rate capability.^[2,12,16,18] First, the hollow structure is often associated with a high surface area, which may provide extra active sites for lithium storage. Second, the hollow cavity is able to provide free space for strain relaxation and volume-change accommodation of the electrode materials during repeated lithium intercalation–deintercalation. As a result, the pulverization of active materials can be alleviated and the cycling performance can be significantly improved. Third, the thin and permeable shells of the hollow structures can provide reduced diffusion distances for both lithium ions and electrons, leading to enhanced rate capability.

TMOs based on the conversion-reaction mechanism possess high specific capacities 2–3 times those of graphite.^[195,196] However, they suffer from large volume expansion during lithiation, which causes pulverization of the active materials and rapid capacity decay during cycling. Constructing TMO intricate hollow structures can effectively address the volume-expansion-associated issues. Ma, Yao, and co-workers performed a comparative study on the lithium-storage performance of Co_3O_4 SSHSs, DSHSs, and TSHSs constructed from nanosheets.^[51] The Co_3O_4 DSHSs exhibit the best cycling performance among the three samples. Even after 50 cycles at 0.2C, a high capacity of 866 mA h g^{-1} can be retained, close to the theoretical capacity of Co_3O_4 (890 mA h g^{-1}). The best cycling performance of the Co_3O_4 DSHSs can be ascribed to the optimized void space for volume-expansion accommodation during lithium uptake. Wang et al. studied the lithium-storage performances of Co_3O_4 SSHSs, DSHSs, TSHSs, and quadruple-shelled hollow spheres (QSHSs) “templated from” carbonaceous microspheres.^[105] Among the four samples, the TSHSs show the highest specific capacity and the best cycling performance. Interestingly, the Co_3O_4 TSHSs deliver an extremely high reversible capacity of $\approx 1620 \text{ mA h g}^{-1}$ after 30 cycles at 50 mA g^{-1} , which is much higher than its theoretical capacity. The extra capacity is attributed to the formation of a solid electrolyte interphase (SEI) film which stores lithium reversibly and the interfacial lithium-storage mechanism.

Iron oxides have also received much attention as conversion-reaction-based LIB anode materials due to their high theoretical capacity, high abundance, low cost, and nontoxicity.^[197] Wang and co-workers reported the synthesis of $\alpha\text{-Fe}_2\text{O}_3$ hollow spheres with controlled shell thickness, shell number, and porosity using carbonaceous spheres as the “hard templates”.^[100] The porous $\alpha\text{-Fe}_2\text{O}_3$ hollow spheres with thin shells outperform those with thick shells in terms of specific capacity and cycling stability. At a current density of 50 mA g^{-1} , the single-, double-, and triple-shelled $\alpha\text{-Fe}_2\text{O}_3$ hollow spheres with thin shells deliver stable capacities of ≈ 1500 , 1600 , and 1700 mA h g^{-1} , respectively. As in the case of Co_3O_4 multishelled hollow spheres, the reversible capacity for $\alpha\text{-Fe}_2\text{O}_3$ multishelled hollow spheres is also observed to be significantly higher than the theoretical capacity (1007 mA h g^{-1}). Enhanced

lithium-storage performances have also been reported for intricate hollow-structured TMOs with other compositions, such as SnO_2 ,^[138] TiO_2 ,^[107] MMn_2O_4 ($\text{M} = \text{Zn}, \text{Co}$),^[76,78] and MCo_2O_4 ($\text{M} = \text{Zn}, \text{Ni}, \text{Mn}$).^[79,94,189] These studies clearly verify the advantages of intricate hollow structures in boosting the lithium-storage performances of TMO-based anode materials.

Compared with anode materials, reports on intricate hollow-structured cathode materials are relatively rare. Xue and co-workers fabricated $\text{V}_2\text{O}_5\text{-SnO}_2$ double-shelled capsules (Figure 17) in which the SnO_2 nanocrystals with a weight percentage of 10 or 15 wt% were homogeneously distributed in a V_2O_5 matrix.^[164] Interestingly, the $\text{V}_2\text{O}_5\text{-SnO}_2$ double-shelled capsules can act as both the cathode and anode materials for LIBs. As the anode material for LIBs (0.01–3.0 V), the $\text{V}_2\text{O}_5\text{-SnO}_2$ double-shelled capsules deliver a reversible capacity of 947 mA h g^{-1} at 250 mA g^{-1} , remaining at 673 mA h g^{-1} after 50 cycles. As the cathode material for LIBs (2.0–3.0 V), the composite capsules deliver a reversible capacity of 212 mA h g^{-1} at 100 mA g^{-1} , maintaining at 174 mA h g^{-1} after 50 cycles.

LiMn_2O_4 spinel is one of the most promising cathode materials for LIBs due to its low cost, the resources of Mn, its low toxicity, high safety, and 3D channels for rapid lithium-ion diffusion. Xie and co-workers prepared LiMn_2O_4 DSHSs using MnCO_3 as the precursor.^[198] The LiMn_2O_4 DSHSs deliver a specific capacity of 127 mA h g^{-1} at 0.1C ($1\text{C} = 120 \text{ mA h g}^{-1}$ for LiMn_2O_4) and a high capacity retention of 80% after 800 cycles at 5C. LiMn_2O_4 multishelled hollow spheres with superior electrochemical performances have also been reported by Sim and co-workers^[145] and Li and co-workers^[199] via spray pyrolysis. $\text{LiNi}_{0.5}\text{Mn}_{1.5}\text{O}_4$ is another type of spinel cathode. With a high operating voltage of $\approx 4.7 \text{ V}$ and a practical capacity of $\approx 140 \text{ mA h g}^{-1}$, $\text{LiNi}_{0.5}\text{Mn}_{1.5}\text{O}_4$ is able to deliver an energy density as high as 658 W h kg^{-1} , which is 20–30% higher than those of conventional LiCoO_2 , LiFePO_4 , and LiMn_2O_4 . Choi et al. reported the spray-pyrolysis synthesis of $\text{LiNi}_{0.5}\text{Mn}_{1.5}\text{O}_4$ multishelled hollow spheres, which deliver a specific capacity of 108 mA h g^{-1} after 1000 cycles at 10C ($1\text{C} = 148 \text{ mA h g}^{-1}$ for $\text{LiNi}_{0.5}\text{Mn}_{1.5}\text{O}_4$).^[151]

4.2. Lithium–Sulfur Batteries

Li–S batteries have been considered as one of the most promising candidates for next-generation rechargeable batteries.^[200–202] They have attractive features such as: i) the natural abundance and low cost of S, and ii) a high theoretical gravimetric and volumetric energy density. Despite their multiple merits, Li–S batteries have not reached mass commercialization even after decades of development. The key challenges facing Li–S batteries include: i) the electronic/ionic insulating nature of S and its discharge products (Li_2S and Li_2S_2), which lead to low active-material utilization and poor rate capability; ii) the dissolution and shuttling of polysulfides in a liquid electrolyte, which result in fast capacity fading and low Coulombic efficiency; and iii) the large volume expansion of S during lithiation, which renders poor cycling performance.

Many efforts to improve the electrochemical performances of Li–S batteries have been focusing on the development of S-based cathode materials, especially carbon–sulfur composites. Among the various carbon materials, hollow carbon spheres are particularly attractive due to the following advantages: i) hollow

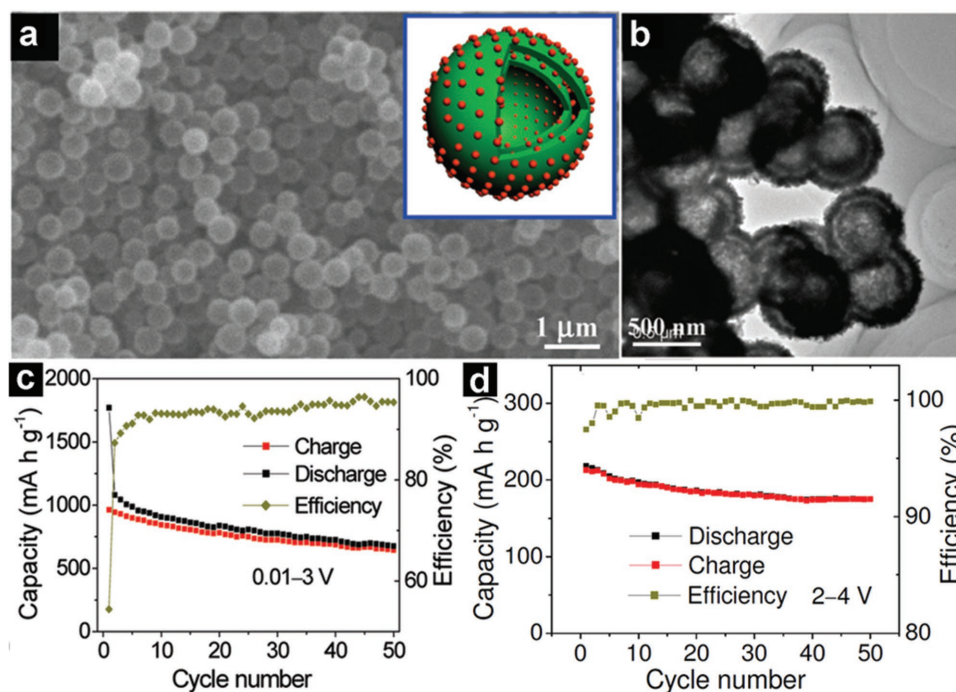


Figure 17. a,b) SEM (a) and TEM (b) images of the V_2O_5 - SnO_2 double-shelled capsules. c) Cycling performance of the V_2O_5 - SnO_2 double-shelled capsules in the potential window of 0.01–3.0 V. d) Cycling performance of the V_2O_5 - SnO_2 double-shelled capsules in the potential window of 2.0–4.0 V. Reproduced with permission.^[164] Copyright 2009, American Chemical Society.

carbon spheres can host large amounts of S; ii) with an optimized loading amount, hollow carbon spheres can provide sufficient free space to accommodate the volume variation of S during lithiation/delithiation; iii) the shell of the hollow carbon spheres can act as a physical barrier to effectively suppress the dissolution and shuttling of polysulfides in the electrolyte; iv) the pores on the shell of the hollow carbon spheres can ensure good accessibility of lithium ions to the loaded S; and v) hollow carbon spheres with high electric conductivity can wire (i.e., improve the conductivity of) the S, improving its utilization. Considering the physical barrier effect of the shell, multishelled hollow carbon spheres may outperform their single-shelled counterparts in S hosting. Lou, Guo, and co-workers designed double-shelled hollow carbon spheres using SnO_2 hollow spheres as the template and encapsulated S in such complex hollow structures.^[39] The resultant carbon-sulfur composite delivers an initial discharge capacity of 1020 $mA\ h\ g^{-1}$ at 0.1C (1C = 1675 $mA\ h\ g^{-1}$ for S), maintaining at 690 $mA\ h\ g^{-1}$ after 100 cycles. Wang and co-workers prepared multishell hollow carbon vesicles through an aqueous emulsion approach and encapsulated a high amount of S (86 wt%) in the multishell vesicles.^[203] The as-obtained carbon-sulfur composite delivers high specific capacities of 1350 and 1003 $mA\ h\ g^{-1}$ at 0.1C and 1C, respectively. After 200 cycles, specific capacities of 1250 and 846 $mA\ h\ g^{-1}$ can be retained at 0.1C and 1C, respectively. The high specific capacity, good rate capability, and excellent cyclability promise the utilization of multishell hollow carbon structures in S hosting for Li-S batteries.

Manthiram and co-workers designed a free-standing and flexible S-based cathode by encapsulating S in N-doped double-shelled hollow carbon spheres followed by graphene

wrapping.^[41] The flexible electrode without any binder delivers a high specific capacity (1360 $mA\ h\ g^{-1}$ at 0.2C), excellent rate capability (600 $mA\ h\ g^{-1}$ at 2C), and long cycle life. The excellent electrochemical performance is attributed to the dual-protected strategy. Specifically, i) the double-shelled hollow carbon spheres provide high porosity for S loading and volume-change accommodation, and effective physical confinement for S and polysulfide, as well as high conductivity for electron transfer; ii) the porous shells of the double-shelled hollow carbon spheres facilitate electrolyte permeation and rapid ion diffusion; iii) the graphene enables the construction of flexible electrodes; and iv) the heteroatoms (N) provide relatively strong affinity to polysulfides through chemical binding, suppressing polysulfide dissolution, and active material loss.

Although the dissolution of polysulfides in electrolyte can be mitigated by applying porous carbon materials as the hosts, the interaction (physical adsorption) between the nonpolar carbon and polar polysulfides is relatively weak. It can be expected that polar host materials showing strong interactions with polysulfide species would outperform nonpolar carbon materials in suppressing polysulfide dissolution and achieving long-term cycling stability. Recently, Lou and co-workers designed $Co(OH)_2@Ni-Co$ LDH DSNCs as a novel S host for Li-S batteries.^[166] Due to the high porosity, the $Co(OH)_2@Ni-Co$ LDH DSNCs can be loaded with a large amount of S (75 wt%). In addition, the $Co(OH)_2@Ni-Co$ LDH/S composite delivers a high initial discharge capacity of 1014 $mA\ h\ g^{-1}$ at 0.1C with excellent cycling stability. The concept of using multishell hollow-structured metal hydroxides or oxides in S hosting will open a new avenue for the future development of high-performance Li-S batteries.

4.3. Supercapacitors

Supercapacitors are a unique class of electrochemical energy-storage device with high power density (10 kW kg^{-1}), ultrafast charge/discharge rate (a few seconds), and long cycle life (100 000 cycles). With a moderate energy density (5 W h kg^{-1}), supercapacitors can bridge the gap between conventional dielectric capacitors and secondary batteries. They have played an important role in complementing or replacing secondary batteries in energy storage.^[204] According to the charge-storage mechanism, supercapacitors can be classified into: i) electrical-double-layer capacitors (EDLCs), ii) pseudocapacitors, and iii) hybrid capacitors. EDLCs store charge electrostatically through reversible ion adsorption at interfaces between a high-surface-area electrode (usually carbon) and the electrolyte. Pseudocapacitors store charge Faradaically using fast and reversible surface or near-surface redox reactions. Hybrid capacitors combine a capacitive or pseudocapacitive active material with a battery active material.

TMOs, such as RuO_2 , CoO_x , NiO , MnO_x , and NiCo_2O_4 , are typical pseudocapacitive active materials. Yu, Wang, and co-workers reported the fabrication of uniform single-, double-, triple-, and quadruple-shelled Mn_2O_3 hollow spheres and evaluated these hollow structures as electrodes for supercapacitors.^[108] Impressively, high specific capacitances of 1651 and 1422 F g^{-1} can be achieved for the Mn_2O_3 TSHSs at current densities of 0.5 and 10 A g^{-1} , respectively. After 2000 cycles at 0.5 A g^{-1} , 92% of the capacitance can be retained. The high specific capacitance and excellent rate performance can be ascribed to the high specific surface area and porosity, which guarantee an abundance of active sites and easy electrolyte penetration. Lou and co-workers designed $\text{Co}_3\text{O}_4@\text{NiCo}_2\text{O}_4$ DSNCs with a rhombic dodecahedral shape.^[92] The as-obtained $\text{Co}_3\text{O}_4@\text{NiCo}_2\text{O}_4$ delivers high specific capacitances of 972, 870 and 615 F g^{-1} at high current densities of 5, 10 and 50 A g^{-1} , respectively. At a current density of 10 A g^{-1} , 92.5% of the initial capacitance can be maintained after 12 000 cycles, demonstrating the excellent cyclability. Superior pseudocapacitive performances have also been demonstrated for Co_3O_4 ,^[113] NiO ,^[114] and CoNi_2O_4 ^[79] multishell hollow spheres, justifying the advantages of intricate hollow structures in supercapacitors.

Metal sulfides can be used as battery-type electrodes in hybrid capacitors in alkaline solution according to the following reversible redox reaction: $\text{MS} + \text{OH}^- \leftrightarrow \text{MSOH} + \text{e}^-$ ($\text{M} = \text{Ni}, \text{Co}, \text{Cu}, \text{and Mn}$).^[18] Lou and co-workers developed a general template-engaged strategy for the fabrication of NiS, CuS, and MnS double-shelled box-in-box hollow structures.^[165] The resultant NiS box-in-box hollow structures display high specific capacitance (668 F g^{-1} at a current density of 1 A g^{-1}), excellent rate capability (71% capacitance retention at 20 A g^{-1}), and good cycling stability (93.4% capacitance retention after 3000 cycles at 4 A g^{-1}). In addition to binary metal sulfides, the same group also prepared ternary metal sulfides (NiCo_2S_4 and MnCo_2S_4) with complex double-shelled hollow structures.^[73] As a typical battery-like electrode, the NiCo_2S_4 DSHSs deliver a high

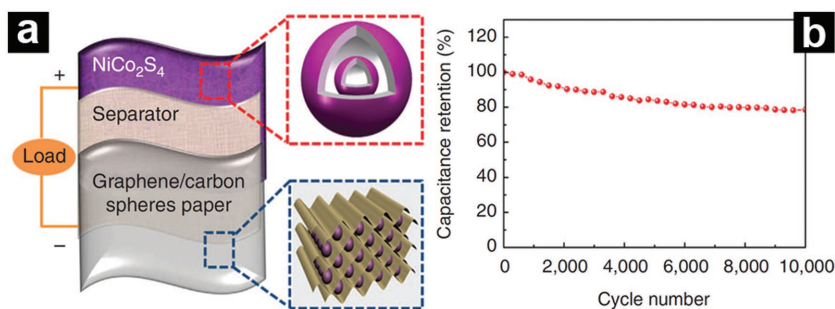


Figure 18. a) Schematic illustration of the NiCo_2S_4 //graphene/carbon sphere paper asymmetric supercapacitor device. b) Cycling performance of the asymmetric supercapacitor device at a current density of 5 A g^{-1} . Reproduced with permission.^[73] Copyright 2014, Nature Publishing Group.

specific capacitance of 1036 F g^{-1} at 1 A g^{-1} . A hybrid capacitor device was fabricated using the NiCo_2S_4 DSHSs as the cathode and a graphene/mesoporous-carbon sphere composite paper as the anode (Figure 18). The hybrid-capacitor device displays a high energy density of 42.3 W h kg^{-1} at a power density of 476 W kg^{-1} . High cycling stability is also achieved by the hybrid capacitor; 78.6% of the initial capacitance can be maintained after 10 000 cycles at 5 A g^{-1} .

4.4. Lithium–Air Batteries

The Li-O_2 battery is a promising technology for energy storage despite being in its infancy of understanding. In theory, such a battery is able to deliver an extremely high energy density of $\approx 3500 \text{ W h kg}^{-1}$ (based on the mass of Li and O_2), although it is far from being reached currently.^[201] However, several critical fundamental challenges still hamper the practical realization of Li-O_2 batteries. One of the main concerns is related to the inherent sluggish kinetics of oxygen-involved electrocatalysis, such as oxygen-reduction reaction (ORR) and oxygen-evolution reaction (OER).

Intricate hollow-structured electrocatalysts, such as transition metals, TMOs, and transition-metal sulfides, have been demonstrated to be highly active in the ORR or the OER.^[92,93,189] As an example, the $\text{Co-C}@Co_9S_8$ DSNCs exhibit an ORR onset potential of 0.96 V (vs reversible hydrogen electrode (RHE)) with the cathodic peak centered at 0.83 V.^[93] Both the onset potential and cathodic peak potential of $\text{Co-C}@Co_9S_8$ DSNCs are very close to those of a commercial 20 wt% Pt/C catalyst. The high activity can be ascribed to the unique DSNC structure, in which the inner Co-C shell acts as the active centers to efficiently catalyze the ORR, while the outer Co_9S_8 shell builds up a nanoreactor around the Co-C catalyst and prevents it from deactivation.

More interestingly, intricate hollow-structured TMOs can also act as efficient bifunctional catalysts for Li-O_2 batteries. The CoMn_2O_4 tube-in-tube structures prepared by electrospinning have been explored as the cathode catalyst in Li-O_2 cells by Chen, Ramakrishna, and co-workers.^[185] With the help of the CoMn_2O_4 tube-in-tube catalyst, the hysteresis between the charge and discharge can be significantly reduced from 1.82 V to 1.2 V. Under a restricting capacity of 1000 mA h g^{-1}

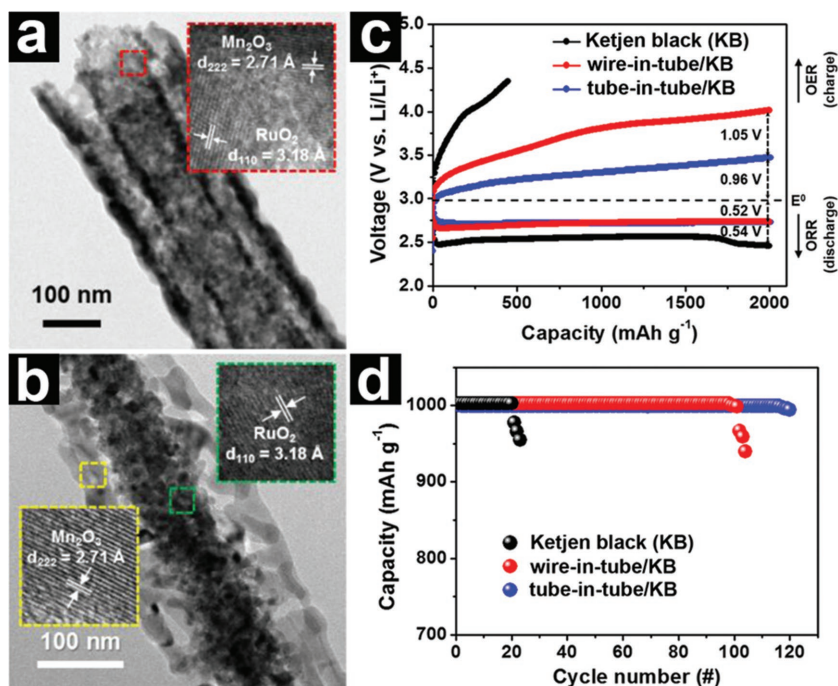


Figure 19. a,b) TEM images of RuO₂/Mn₂O₃ tube-in-tube (a) and wire-in-tube (b) structures. c) First discharge–charge curves of Ketjen black, RuO₂/Mn₂O₃ tube-in-tube structure, and RuO₂/Mn₂O₃ wire-in-tube structure with a capacity limit of 2000 mA h g⁻¹ at a current density of 100 mA g⁻¹ with a voltage window of 2.35–4.35 V. d) Their cycling performances. Reproduced with permission.^[205] Copyright 2016, American Chemical Society.

(based on the mass of carbon), the cell based on the CoMn₂O₄ tube-in-tube catalyst can be discharged and charged stably at 200 mA g⁻¹ for at least 100 cycles. In another case, Kim and co-workers fabricated RuO₂/Mn₂O₃ composite tube-in-tube and wire-in-tube hollow structures (Figure 19a,b).^[205] In the constructed composites, Mn₂O₃ is active for both the ORR (major) and the OER (minor), and RuO₂ is mainly active for the OER. As a result, the RuO₂/Mn₂O₃ composite hollow structures exhibit excellent electrocatalytic performances for the ORR and the OER in both alkaline media and Li–O₂ cells. With a capacity restriction of 2000 mA h g⁻¹ (based on the total mass of the catalysts and carbon), the Li–O₂ cell based on a RuO₂/Mn₂O₃ cathode displays a voltage gap of 1.48 V (Figure 19c). By limiting the discharge capacity to 1000 mA h g⁻¹, cells based on the RuO₂/Mn₂O₃ tube-in-tube and wire-in-tube hollow structures can be cycled stably for over 100 cycles (Figure 19d).

4.5. Dye-Sensitized Solar Cells

DSSCs consisting of a dye-sensitized nanocrystalline and porous photoanode, a redox-active liquid electrolyte, and a counter electrode, are a promising photoelectrochemical system for efficient solar-energy conversion.^[206] An ideal photoanode for DSSCs should have a large surface area for dye absorbing and excellent light-harvesting capability. Hollow structures, especially intricate hollow structures, have been considered as promising photoanode materials for DSSCs. Cao and co-workers reported the design of TiO₂-coated multishell SnO₂ hollow spheres as an advanced photoanode material for

DSSCs.^[207] A cell based on a photoanode made from these TiO₂-coated multishell SnO₂ hollow spheres exhibited an overall conversion efficiency of ≈5.65%, which is 34% higher than that of the cell based on a TiO₂-coated SnO₂ nanoparticle photoanode (Figure 20). The improvement is tentatively attributed to the multiple light reflection and scattering in-between different shells. This work highlights the advantages of MSHSs in light harvesting.

The concept of designing intricate hollow structures to enhance the light-harvesting capability of semiconductor photoanodes has also been adopted by other groups. Lu, Wang, and co-workers prepared TiO₂ DSHSs by a facile hydrothermal method followed by calcination in air.^[119] As the photoanode for DSSCs, the TiO₂ DSHSs display an overall photoconversion efficiency of 5.65%. By employing the TiO₂ DSHSs as the light-scattering layer over the P25 films, an overall photoconversion efficiency of 9.10% can be achieved. Li, Shi, and co-workers fabricated coaxial multishell TiO₂ nanotube arrays on a transparent conductive oxide substrate.^[208] The specific Brunauer–Emmett–Teller (BET) surface area and the amount of dye adsorbed increases with the increase of shell number.

As a result, the DSSC performance also increases with the increase of shell number. A maximum conversion efficiency of 6.2% is achieved for the quintuple-shelled TiO₂ nanotube photoanode. Wang and co-workers fabricated a series of ZnO and SnO₂ hollow spheres with controlled number of shells and intershell spacings.^[101,106] It was found that the multishell

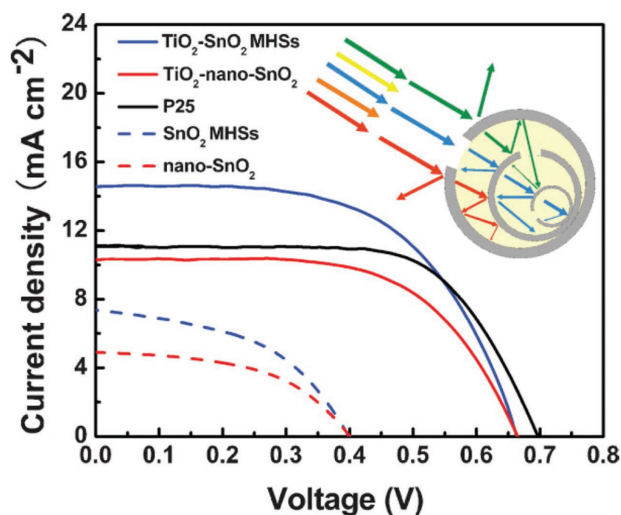


Figure 20. Current–voltage characteristics of DSSCs based on photoelectrode films of TiO₂-coated multishelled SnO₂ hollow spheres, TiO₂-coated SnO₂ nanoparticles, P25, multishell SnO₂ hollow spheres, and SnO₂ nanoparticles. The inset illustrates the multiple reflecting and scattering of light in the multishell SnO₂ hollow sphere. Reproduced with permission.^[207]

hollow spheres provide more surface area for dye absorption and enable multiple light reflection and scattering in-between the different shells. As a result, the overall energy-conversion efficiency increases with the number of shells in both cases. DSSCs based on a ZnO QSHS photoanode exhibit an overall conversion efficiency of 5.6%, while the cells based on SnO₂ quintuple-shelled hollow spheres exhibit a efficiency of 7.18%. When the SnO₂ quintuple-shelled hollow spheres are used as the scattering layer on top of P25 film, the overall conversion efficiency can reach as high as 9.53%. Recently, Jang and co-workers prepared TiO₂ SSHSs, DSHSs, and TSHSs using a shell-by-shell deposition process combined with calcination and selective etching.^[25] Among the three TiO₂ samples with different shell numbers, the TSHSs show the highest power conversion efficiency of 9.4%. Using a similar approach, the same group also prepared SiO₂/TiO₂ DSHSs.^[26] Using the SiO₂/TiO₂ DSHSs as the light scattering layer, the assembled DSSC exhibits a power conversion efficiency of 8.4%.

4.6. Photocatalysis

Photocatalysis has become an emerging technology using solar energy for water and air purification and remediation since Fujishima and Honda first discovered photocatalytic splitting of water on TiO₂ in 1972.^[209] One of the most prominent advantages of intricate hollow structures in photocatalysis is that they allow multiple reflections of the incident light, resulting in enhanced light-harvesting efficiency and thus enhanced photocatalytic performances.^[16] Early in 2007, Li, Lu, and co-workers found that sphere-in-sphere-structured TiO₂ could allow multiple reflections of UV light, resulting in significantly enhanced photocatalytic activity in phenol degradation.^[210] Yao and co-workers fabricated multishell TiO₂ hollow spheres that displayed much higher photocatalytic activity in Rhodamine B (RhB) degradation than the TiO₂ yolk-shell structures and nanoparticles.^[22] Zhao et al. reported the fabrication of Fe₃O₄@titanate core-in-double-shell spheres by a hydrothermal-etching-assisted crystallization approach.^[211] The resulting Fe₃O₄@titanate hollow structures showed excellent photocatalytic activity toward RhB degradation, which was superior to that of P25 TiO₂. Because of the magnetic core, the photocatalyst can be easily recovered and recycled, exhibiting almost constant activity after 10 cycles. Apart from the above-mentioned studies, intricate hollow-structured ZnO,^[122,190,212] Fe₂O₃,^[116] WO₃,^[110] CeO₂,^[124] Zn-Sn-O,^[65] and Cu₉S₅^[213] have also been demonstrated to be effective in the photocatalytic degradation of organic dyes and water splitting.

4.7. Fuel Cells

Fuel cells are energy-conversion devices that convert the chemical energy of a fuel, such as hydrogen, methanol, and ethanol, into electricity. The electricity is generated through the electrochemical catalytic oxidation of a fuel at the anode and reduction of oxygen at the cathode.^[214] The performance of fuel cells is highly dependant on their electrocatalysts. Noble-metal nanoparticles supported on carbon are well-known electrocatalysts

for fuel cells. Due to the high surface area, high pore volume, low density, and reduced mass- and charge-diffusion lengths, hollow structures have been considered as promising electrocatalysts and catalyst supports for fuel cells.^[215–220] Wang and Yamauchi fabricated bimetallic Pt-Pd nanocages with dendritic shells via a selective chemical etching method.^[217] Benefiting from their sufficient accessible active sites at both the exterior and interior surfaces, the resultant Pt-Pd nanocages exhibited high catalytic activity toward methanol oxidation. As for the catalyst supports, Yu and co-workers reported the hard-templating synthesis of mesoporous-carbon capsules with high specific surface area and pore volume. The obtained mesoporous-carbon capsules are able to support ultrafine noble-metal nanoparticles uniformly, boosting the performance of fuel cells.^[219,220]

5. Conclusion and Perspectives

Here, we have highlighted the most important synthetic methodologies and energy applications of intricate hollow structures. Significant advances have been made in the synthesis of intricate hollow structures in the last decade, with a number of new synthetic methodologies emerging. These emerging synthetic methodologies include selective etching of “soft@hard” particles, Ostwald ripening, ion exchange, and thermally induced matter relocation. For future research in the synthesis of intricate hollow structures, we believe that it should concentrate on the following aspects:

- i) Both conventional and newly emerging methodologies suffer from one or more of the following deficiencies: troublesome synthesis procedure, difficulty in precise control, lack of uniformity and universality, unfeasible for mass production, high cost, and poorly understood formation mechanism. In this regard, the development of facile, versatile, low-cost, and scalable approaches for the production of high-quality intricate hollow structures with tunable compositions and precisely controlled structural parameters is of primary importance.
- ii) To date, most studies of intricate hollow structures have focused on native elements, oxides, and sulfides, while complex hollow-structured carbides, nitrides, phosphides, and selenides have rarely been reported. Given their unique physicochemical properties, the fabrication of complex hollow-structured carbides, nitrides, phosphides, and selenides is of great significance.
- iii) A number of intricate hollow structures are prepared by accidental windfalls or relying on the experiences of researchers. The rational design of intricate hollow structures for specific applications remains a great challenge and should be strengthened in the future.
- iv) The formation mechanism of some intricate hollow structures remains elusive. It would be very helpful to deepen the comprehension and understanding of the formation mechanism, which would spur novel and powerful methodologies for intricate hollow structure construction.

The breakthroughs in synthetic methodologies for intricate hollow structures have provided opportunities to tune their physicochemical properties and have thus catalyzed their

exploration in various applications. Although intricate hollow structures have been extensively studied in LIBs, their application in sodium-ion batteries (SIBs) has attracted little attention. Considering the large ionic radius of Na⁺ and large free space required for Na⁺ accommodation, we expect to see a surge in the application of such unique structures in SIBs in the near future. The major issue of employing hollow structures in LIBs and supercapacitors is their low density, which will compromise the volumetric energy density of the devices. In this case, optimizing the void-to-solid ratio of the intricate hollow structures is required to maximize the volumetric energy density without sacrificing the cyclability. For Li–S battery applications, intricate hollow structures with both high conductivity and high affinity to polysulfides are preferred. Multicomponent intricate hollow structures with high activity toward both the ORR and the OER would play a significant role in Li–O₂ batteries. More efforts dedicated to the structural manipulation, such as shell-number control and intershell-spacing adjustment, would further boost the performance of intricate hollow-structured semiconductors in DSSCs and photocatalysis.

Lastly, it should be emphasized that the synthesis and energy applications of intricate hollow structures is still in its infancy. There is still a long way to go for the commercial-scale production and practical application of such intriguing materials. Although we have summarized some recent work on the synthesis and energy applications of intricate hollow structures, we would rather regard this review as an opening remark than a concluding remark. We are confident that other versatile and powerful synthetic methodologies for intricate hollow structures will be developed in the near future. We also believe that intricate hollow structures will break some of the current bottlenecks in the fields of energy storage and conversion.

Acknowledgements

This work was supported by the National Key Research and Development Program of China (2016YFA0202603), the National Basic Research Program of China (2013CB934103), the Programme of Introducing Talents of Discipline to Universities (B17034), the National Natural Science Foundation of China (51502226, 21673171, 51521001, 51272197), the National Natural Science Fund for Distinguished Young Scholars (51425204), the Hubei Provincial Natural Science Fund for Distinguished Young Scholars (2014CFA035), and the Fundamental Research Funds for the Central Universities (WUT: 152401004, 2015111022, 20161VA091, 2016111001, 2016111002). The authors thank Prof. C. M. Liber at Harvard University for the strong support and stimulating discussions.

Received: June 2, 2016

Revised: November 5, 2016

Published online:

- [1] C. C. Yec, H. C. Zeng, *J. Mater. Chem. A* **2014**, *2*, 4843.
 [2] X. W. Lou, L. A. Archer, Z. C. Yang, *Adv. Mater.* **2008**, *20*, 3987.
 [3] Y. Zhao, L. Jiang, *Adv. Mater.* **2009**, *21*, 3621.
 [4] K. An, T. Hyeon, *Nano Today* **2009**, *4*, 359.
 [5] J. Liu, F. Liu, K. Gao, J. S. Wu, D. F. Xue, *J. Mater. Chem.* **2009**, *19*, 6073.

- [6] Q. Zhang, W. S. Wang, J. Goebel, Y. D. Yin, *Nano Today* **2009**, *4*, 494.
 [7] K. Cheng, S. H. Sun, *Nano Today* **2010**, *5*, 183.
 [8] J. Hu, M. Chen, X. S. Fang, L. W. Wu, *Chem. Soc. Rev.* **2011**, *40*, 5472.
 [9] X. Y. Lai, J. E. Halpert, D. Wang, *Energy Environ. Sci.* **2012**, *5*, 5604.
 [10] Z. Wang, L. Zhou, X. W. Lou, *Adv. Mater.* **2012**, *24*, 1903.
 [11] M. Chen, C. Y. Ye, S. X. Zhou, L. M. Wu, *Adv. Mater.* **2013**, *25*, 5343.
 [12] W. Wei, Z. H. Wang, Z. Liu, Y. Liu, L. He, D. Z. Chen, A. Umar, L. Guo, J. H. Li, *J. Power Sources* **2013**, *238*, 376.
 [13] Y. Chen, H. R. Chen, J. L. Shi, *Acc. Chem. Res.* **2014**, *47*, 125.
 [14] J. Lee, S. M. Kim, I. S. Lee, *Nano Today* **2014**, *9*, 631.
 [15] Y. S. Li, J. L. Shi, *Adv. Mater.* **2014**, *26*, 3176.
 [16] J. Qi, X. Y. Lai, J. Y. Wang, H. J. Tang, H. Ren, Y. Yang, Q. Jin, L. J. Zhang, R. B. Yu, G. H. Ma, Z. G. Su, H. J. Zhao, D. Wang, *Chem. Soc. Rev.* **2015**, *44*, 6749.
 [17] Y. S. Si, M. Chen, L. M. Wu, *Chem. Soc. Rev.* **2016**, *45*, 690.
 [18] X. Y. Yu, L. Yu, X. W. Lou, *Adv. Energy Mater.* **2016**, *6*.
 [19] X. J. Wang, J. Feng, Y. C. Bai, Q. Zhang, Y. D. Yin, *Chem. Rev.* **2016**, *116*, 10983.
 [20] W. S. Wang, M. Dahl, Y. D. Yin, *Chem. Mater.* **2013**, *25*, 1179.
 [21] H. C. Zeng, *J. Mater. Chem.* **2011**, *21*, 7511.
 [22] Y. Zeng, X. Wang, H. Wang, Y. Dong, Y. Ma, J. N. Yao, *Chem. Commun.* **2010**, *46*, 4312.
 [23] F. Caruso, R. A. Caruso, H. Mohwald, *Science* **1998**, *282*, 1111.
 [24] W. Stober, A. Fink, *J. Colloid Interface Sci.* **1968**, *26*, 62.
 [25] S. H. Hwang, J. Yun, J. Jang, *Adv. Funct. Mater.* **2014**, *24*, 7619.
 [26] J. Lee, S. H. Hwang, J. Yun, J. Jang, *ACS Appl. Mater. Interfaces* **2014**, *6*, 15420.
 [27] S. Lee, J. Lee, S. H. Hwang, J. Yun, J. Jang, *ACS Nano* **2015**, *9*, 4939.
 [28] G. L. Li, Q. Shi, S. J. Yuan, K. G. Neoh, E. T. Kang, X. L. Yang, *Chem. Mater.* **2010**, *22*, 1309.
 [29] S. S. Cao, Z. Y. Zhao, X. Jin, W. C. Sheng, S. J. Li, Y. Ge, M. D. Dong, W. W. Wu, L. Fang, *J. Mater. Chem.* **2011**, *21*, 19124.
 [30] J. Liu, S. Z. Qiao, H. Liu, J. Chen, A. Orpe, D. Y. Zhao, G. Q. Lu, *Angew. Chem., Int. Ed.* **2011**, *50*, 5947.
 [31] A. B. Fuertes, P. Valle-Vigon, M. Sevilla, *Chem. Commun.* **2012**, *48*, 6124.
 [32] H. Zhang, M. Yu, H. Song, O. Noonan, J. Zhang, Y. Yang, L. Zhou, C. Yu, *Chem. Mater.* **2015**, *27*, 6297.
 [33] J. Zang, J. C. Ye, X. L. Fang, X. W. Zhang, M. S. Zheng, Q. F. Dong, *Electrochim. Acta* **2015**, *186*, 436.
 [34] X. W. Lou, C. L. Yuan, L. A. Archer, *Small* **2007**, *3*, 261.
 [35] J. W. Liu, J. Cheng, R. C. Che, J. J. Xu, M. M. Liu, Z. W. Liu, *J. Phys. Chem. C* **2013**, *117*, 489.
 [36] X. W. Lou, C. L. Yuan, L. A. Archer, *Adv. Mater.* **2007**, *19*, 3328.
 [37] M. Yang, J. Ma, C. L. Zhang, Z. Z. Yang, Y. F. Lu, *Angew. Chem., Int. Ed.* **2005**, *44*, 6727.
 [38] M. Yang, J. Ma, Z. W. Niu, X. Dong, H. F. Xu, Z. K. Meng, Z. G. Jin, Y. F. Lu, Z. B. Hu, Z. Z. Yang, *Adv. Funct. Mater.* **2005**, *15*, 1523.
 [39] C. F. Zhang, H. B. Wu, C. Z. Yuan, Z. P. Guo, X. W. Lou, *Angew. Chem., Int. Ed.* **2012**, *51*, 9592.
 [40] K. L. Zhang, X. N. Li, J. W. Liang, Y. C. Zhu, L. Hu, Q. S. Cheng, C. Guo, N. Lin, Y. T. Qian, *Electrochim. Acta* **2015**, *155*, 174.
 [41] G. M. Zhou, Y. B. Zhao, A. Manthiram, *Adv. Energy Mater.* **2015**, *5*.
 [42] R. Pang, X. J. Hu, S. Y. Zhou, C. H. Sun, J. Yan, X. M. Sun, S. Z. Xiao, P. Chen, *Chem. Commun.* **2014**, *50*, 12493.
 [43] Z. Sun, X. F. Song, P. Zhang, L. Gao, *RSC Adv.* **2015**, *5*, 3657.
 [44] S. S. Kim, W. Z. Zhang, T. J. Pinnavaia, *Science* **1998**, *282*, 1302.
 [45] J. Liu, S. B. Hartono, Y. G. Jin, Z. Li, G. Q. Lu, S. Z. Qiao, *J. Mater. Chem.* **2010**, *20*, 4595.
 [46] Y. Zhang, M. Yu, L. Zhou, X. Zhou, Q. Zhao, H. Li, C. Yu, *Chem. Mater.* **2008**, *20*, 6238.

- [47] D. Gu, H. Bongard, Y. H. Deng, D. Feng, Z. X. Wu, Y. Fang, J. J. Mao, B. Tu, F. Schuth, D. Y. Zhao, *Adv. Mater.* **2010**, *22*, 833.
- [48] J. Liu, T. Y. Yang, D. W. Wang, G. Q. M. Lu, D. Y. Zhao, S. Z. Qiao, *Nat. Commun.* **2013**, *4*.
- [49] H. L. Xu, W. Z. Wang, *Angew. Chem., Int. Ed.* **2007**, *46*, 1489.
- [50] W. Z. Wang, Y. Tu, P. C. Zhang, G. L. Zhang, *CrystEngComm* **2011**, *13*, 1838.
- [51] X. Wang, X. L. Wu, Y. G. Guo, Y. T. Zhong, X. Q. Cao, Y. Ma, J. N. Yao, *Adv. Funct. Mater.* **2010**, *20*, 1680.
- [52] X. Wang, Y. T. Zhong, T. Y. Zhai, Y. F. Guo, S. M. Chen, Y. Ma, J. N. Yao, Y. Bando, D. Golberg, *J. Mater. Chem.* **2011**, *21*, 17680.
- [53] Q. Zhang, T. R. Zhang, J. P. Ge, Y. D. Yin, *Nano Lett.* **2008**, *8*, 2867.
- [54] D. Chen, L. L. Li, F. Q. Tang, S. O. Qi, *Adv. Mater.* **2009**, *21*, 3804.
- [55] X. J. Wu, D. S. Xu, *Adv. Mater.* **2010**, *22*, 1516.
- [56] Z. G. Teng, X. D. Su, Y. Y. Zheng, J. Sun, G. T. Chen, C. C. Tian, J. D. Wang, H. Li, Y. N. Zhao, G. M. Lu, *Chem. Mater.* **2013**, *25*, 98.
- [57] Z. G. Teng, S. J. Wang, X. D. Su, G. T. Chen, Y. Liu, Z. M. Luo, W. Luo, Y. X. Tang, H. X. Ju, D. Y. Zhao, G. M. Lu, *Adv. Mater.* **2014**, *26*, 3741.
- [58] Y. J. Wong, L. F. Zhu, W. S. Teo, Y. W. Tan, Y. H. Yang, C. Wang, H. Y. Chen, *J. Am. Chem. Soc.* **2011**, *133*, 11422.
- [59] Z. G. Teng, X. D. So, Y. Y. Zheng, J. J. Zhang, Y. Liu, S. J. Wang, J. Wu, G. T. Chen, J. D. Wang, D. Y. Zhao, G. M. Lu, *J. Am. Chem. Soc.* **2015**, *137*, 7935.
- [60] C. C. Huang, W. Huang, C. S. Yeh, *Biomaterials* **2011**, *32*, 556.
- [61] L. F. Tan, T. L. Liu, L. L. Li, H. Y. Liu, X. L. Wu, F. P. Gao, X. L. He, X. W. Meng, D. Chen, F. Q. Tang, *RSC Adv.* **2013**, *3*, 5649.
- [62] L. L. Wang, K. B. Tang, Z. P. Liu, D. K. Wang, J. Sheng, W. Cheng, *J. Mater. Chem.* **2011**, *21*, 4352.
- [63] Z. Y. Wang, Z. C. Wang, H. B. Wu, X. W. Lou, *Sci. Rep.* **2013**, *3*, 1391.
- [64] Y. T. Ma, Q. S. Xie, X. Liu, Y. C. Zhao, D. Q. Zeng, L. S. Wang, Y. Zheng, D. L. Peng, *Electrochim. Acta* **2015**, *182*, 327.
- [65] L. Q. Sun, X. Han, Z. Jiang, T. T. Ye, R. Li, X. S. Zhao, X. G. Han, *Nanoscale* **2016**, *8*, 12858.
- [66] M. Hu, S. Furukawa, R. Ohtani, H. Sukegawa, Y. Nemoto, J. Reboul, S. Kitagawa, Y. Yamauchi, *Angew. Chem., Int. Ed.* **2012**, *51*, 984.
- [67] M. Hu, A. A. Belik, M. Imura, Y. Yamauchi, *J. Am. Chem. Soc.* **2013**, *135*, 384.
- [68] W. Z. Ostwald, *Phys. Chem.* **1900**, *34*, 495.
- [69] H. G. Yang, H. C. Zeng, *J. Phys. Chem. B* **2004**, *108*, 3492.
- [70] L. Zhang, H. Wang, *J. Phys. Chem. C* **2011**, *115*, 18479.
- [71] C. C. Yec, H. C. Zeng, *Chem. Mater.* **2012**, *24*, 1917.
- [72] S. L. Xiong, H. C. Zeng, *Angew. Chem., Int. Ed.* **2012**, *51*, 949.
- [73] L. F. Shen, L. Yu, H. B. Wu, X. Y. Yu, X. G. Zhang, X. W. Lou, *Nat. Commun.* **2015**, *6*.
- [74] Y. D. Yin, R. M. Rioux, C. K. Erdonmez, S. Hughes, G. A. Somorjai, A. P. Alivisatos, *Science* **2004**, *304*, 711.
- [75] E. Gonzalez, J. Arbiol, V. F. Puntes, *Science* **2011**, *334*, 1377.
- [76] L. Zhou, D. Zhao, X. W. Lou, *Adv. Mater.* **2012**, *24*, 745.
- [77] W. Cho, Y. H. Lee, H. J. Lee, M. Oh, *Adv. Mater.* **2011**, *23*, 1720.
- [78] G. Q. Zhang, L. Yu, H. B. Wu, H. E. Hoster, X. W. Lou, *Adv. Mater.* **2012**, *24*, 4609.
- [79] L. F. Shen, L. Yu, X. Y. Yu, X. G. Zhang, X. W. Lou, *Angew. Chem., Int. Ed.* **2015**, *54*, 1868.
- [80] X. Y. Lai, J. Li, B. A. Korgel, Z. H. Dong, Z. M. Li, F. B. Su, J. A. Du, D. Wang, *Angew. Chem., Int. Ed.* **2011**, *50*, 2738.
- [81] J. G. Guan, F. Z. Mou, Z. G. Sun, W. D. Shi, *Chem. Commun.* **2010**, *46*, 6605.
- [82] L. Zhou, H. Xu, H. Zhang, J. Yang, S. B. Hartono, K. Qian, J. Zou, C. Yu, *Chem. Commun.* **2013**, *49*, 8695.
- [83] L. Zhou, H. B. Wu, T. Zhu, X. W. Lou, *J. Mater. Chem.* **2012**, *22*, 827.
- [84] H. B. Lin, H. B. Rong, W. Z. Huang, Y. H. Liao, L. D. Xing, M. Q. Xu, X. P. Li, W. S. Li, *J. Mater. Chem. A* **2014**, *2*, 14189.
- [85] J. Cao, Y. C. Zhu, L. Shi, L. L. Zhu, K. Y. Bao, S. Z. Liu, Y. T. Qian, *Eur. J. Inorg. Chem.* **2010**, 1172.
- [86] L. Hu, Q. W. Chen, *Nanoscale* **2014**, *6*, 1236.
- [87] L. Zhang, H. B. Wu, X. W. Lou, *J. Am. Chem. Soc.* **2013**, *135*, 10664.
- [88] W. X. Guo, W. W. Sun, Y. Wang, *ACS Nano* **2015**, *9*, 11462.
- [89] J. Shao, Z. M. Wan, H. M. Liu, H. Y. Zheng, T. Gao, M. Shen, Q. T. Qu, H. H. Zheng, *J. Mater. Chem. A* **2014**, *2*, 12194.
- [90] L. Zhang, H. B. Wu, S. Madhavi, H. H. Hng, X. W. Lou, *J. Am. Chem. Soc.* **2012**, *134*, 17388.
- [91] M. Hu, A. A. Belik, M. Imura, K. Mibu, Y. Tsujimoto, Y. Yamauchi, *Chem. Mater.* **2012**, *24*, 2698.
- [92] H. Hu, B. Y. Guan, B. Y. Xia, X. W. Lou, *J. Am. Chem. Soc.* **2015**, *137*, 5590.
- [93] H. Hu, L. Han, M. Z. Yu, Z. Y. Wang, X. W. Lou, *Energy Environ. Sci.* **2016**, *9*, 107.
- [94] J. F. Li, J. Z. Wang, X. Liang, Z. J. Zhang, H. K. Liu, Y. T. Qian, S. L. Xiong, *ACS Appl. Mater. Interfaces* **2014**, *6*, 24.
- [95] X. M. Sun, Y. D. Li, *Angew. Chem., Int. Ed.* **2004**, *43*, 3827.
- [96] X. L. Li, T. J. Lou, X. M. Sun, Y. D. Li, *Inorg. Chem.* **2004**, *43*, 5442.
- [97] X. M. Sun, J. F. Liu, Y. D. Li, *Chem.–Eur. J.* **2006**, *12*, 2039.
- [98] X. M. Sun, Y. D. Li, *Angew. Chem., Int. Ed.* **2004**, *43*, 597.
- [99] Z. M. Li, X. Y. Lai, H. Wang, D. Mao, C. J. Xing, D. Wang, *J. Phys. Chem. C* **2009**, *113*, 2792.
- [100] S. M. Xu, C. M. Hessel, H. Ren, R. B. Yu, Q. Jin, M. Yang, H. J. Zhao, D. Wang, *Energy Environ. Sci.* **2014**, *7*, 632.
- [101] Z. H. Dong, X. Y. Lai, J. E. Halpert, N. L. Yang, L. X. Yi, J. Zhai, D. Wang, Z. Y. Tang, L. Jiang, *Adv. Mater.* **2012**, *24*, 1046.
- [102] Z. Z. Li, Y. Zhang, Z. Z. Chen, E. W. Shi, *J. Inorg. Mater.* **2009**, *24*, 1263.
- [103] L. L. Wang, H. M. Dou, F. Li, J. N. Deng, Z. Lou, T. Zhang, *Sens. Actuators, B* **2013**, *183*, 467.
- [104] L. L. Wang, Z. Lou, T. Fei, T. Zhang, *J. Mater. Chem.* **2011**, *21*, 19331.
- [105] J. Y. Wang, N. L. Yang, H. J. Tang, Z. H. Dong, Q. Jin, M. Yang, D. Kisailus, H. J. Zhao, Z. Y. Tang, D. Wang, *Angew. Chem., Int. Ed.* **2013**, *52*, 6417.
- [106] Z. H. Dong, H. Ren, C. M. Hessel, J. Y. Wang, R. B. Yu, Q. Jin, M. Yang, Z. D. Hu, Y. F. Chen, Z. Y. Tang, H. J. Zhao, D. Wang, *Adv. Mater.* **2014**, *26*, 905.
- [107] H. Ren, R. B. Yu, J. Y. Wang, Q. Jin, M. Yang, D. Mao, D. Kisailus, H. J. Zhao, D. Wang, *Nano Lett.* **2014**, *14*, 6679.
- [108] J. Y. Wang, H. J. Tang, H. Ren, R. B. Yu, J. Qi, D. Mao, H. J. Zhao, D. Wang, *Adv. Sci.* **2014**, *1*, 1400011.
- [109] Y. Wang, S. S. Niu, S. Lu, *Mater. Lett.* **2015**, *158*, 416.
- [110] G. C. Xi, Y. Yan, Q. Ma, J. F. Li, H. F. Yang, X. J. Lu, C. Wang, *Chem.–Eur. J.* **2012**, *18*, 13949.
- [111] J. Y. Wang, H. J. Tang, L. J. Zhang, H. Ren, R. B. Yu, Q. Jin, J. Qi, D. Mao, M. Yang, Y. Wang, P. Liu, Y. Zhang, Y. R. Wen, L. Gu, G. H. Ma, Z. G. Su, Z. Y. Tang, H. J. Zhao, D. Wang, *Nat. Energy* **2016**, *1*, 16050.
- [112] H. S. Qian, G. F. Lin, Y. X. Zhang, P. Gunawan, R. Xu, *Nanotechnology* **2007**, *18*.
- [113] Y. P. Wang, A. Q. Pan, Q. Y. Zhu, Z. W. Nie, Y. F. Zhang, Y. Tang, S. Q. Liang, G. Z. Cao, *J. Power Sources* **2014**, *272*, 107.
- [114] Z. H. Yang, F. F. Xu, W. X. Zhang, Z. S. Mei, B. Pei, X. Zhu, *J. Power Sources* **2014**, *246*, 24.
- [115] G. Q. Zhang, X. W. Lou, *Angew. Chem., Int. Ed.* **2014**, *53*, 9041.
- [116] Y. Liu, C. Y. Yu, W. Dai, X. H. Gao, H. S. Qian, Y. Hu, X. Hu, *J. Alloys Compd.* **2013**, *551*, 440.
- [117] M. M. Titirici, M. Antonietti, A. Thomas, *Chem. Mater.* **2006**, *18*, 3808.
- [118] H. X. Yang, J. F. Qian, Z. X. Chen, X. P. Ai, Y. L. Cao, *J. Phys. Chem. C* **2007**, *111*, 14067.

- [119] X. Wu, G. Q. Lu, L. Z. Wang, *Energy Environ. Sci.* **2011**, *4*, 3565.
- [120] S. L. Li, A. H. Li, R. R. Zhang, Y. Y. He, Y. J. Zhai, L. Q. Xu, *Nano Res.* **2014**, *7*, 1116.
- [121] H. M. Sun, L. M. Wang, D. Q. Chu, Z. C. Ma, A. X. Wang, *Mater. Lett.* **2015**, *140*, 158.
- [122] X. M. Ma, X. T. Zhang, L. Yang, K. Wang, K. Jiang, Z. P. Wei, Y. M. Guo, *CrystEngComm* **2014**, *16*, 7933.
- [123] S. Y. Bie, Y. Q. Zhu, J. M. Su, C. Jin, S. H. Liu, R. Z. Yang, J. Wu, *J. Mater. Chem. A* **2015**, *3*, 22448.
- [124] J. Qi, K. Zhao, G. D. Li, Y. Gao, H. J. Zhao, R. B. Yu, Z. Y. Tang, *Nanoscale* **2014**, *6*, 4072.
- [125] Z. P. Tian, Y. Zhou, Z. D. Li, Q. Liu, Z. G. Zou, *J. Mater. Chem. A* **2013**, *1*, 3575.
- [126] C. Boissiere, D. Grosso, A. Chaumonnot, L. Nicole, C. Sanchez, *Adv. Mater.* **2011**, *23*, 599.
- [127] N. E. Motl, A. K. P. Mann, S. E. Skrabalak, *J. Mater. Chem. A* **2013**, *1*, 5193.
- [128] M. Eslamian, M. Ahmed, N. Ashgriz, *Nanotechnology* **2006**, *17*, 1674.
- [129] C. Z. Yu, L. Zhou, PCT patent WO2014183169, **2014**.
- [130] Z. Padashbarmchi, A. H. Hamidian, H. Zhang, L. Zhou, N. Khorasani, M. Kazemzad, C. Yu, *RSC Adv.* **2015**, *5*, 10304.
- [131] S. H. Choi, Y. C. Kang, *Chem.–Eur. J.* **2014**, *20*, 5835.
- [132] J. M. Won, S. H. Choi, Y. J. Hong, Y. N. Ko, Y. C. Kang, *Sci. Rep.* **2014**, *4*, 5857.
- [133] J. M. Won, J. H. Lee, Y. C. Kang, *Chem.–Eur. J.* **2015**, *21*, 1429.
- [134] G. D. Park, J. H. Lee, J. K. Lee, Y. C. Kang, *Nano Res.* **2014**, *7*, 1738.
- [135] J. W. Yoon, Y. J. Hong, G. D. Park, S. J. Hwang, F. Abdel-Hady, A. A. Wazzan, Y. C. Kang, J. H. Lee, *ACS Appl. Mater. Interfaces* **2015**, *7*, 7717.
- [136] Z. X. Wu, W. D. Wu, W. J. Liu, C. Selomulya, X. D. Chen, D. Y. Zhao, *Angew. Chem., Int. Ed.* **2013**, *52*, 13764.
- [137] S. W. Oh, H. J. Bang, Y. C. Bae, Y. K. Sun, *J. Power Sources* **2007**, *173*, 502.
- [138] Y. J. Hong, M. Y. Son, Y. C. Kang, *Adv. Mater.* **2013**, *25*, 2279.
- [139] M. Y. Son, Y. J. Hong, Y. C. Kang, *Chem. Commun.* **2013**, *49*, 5678.
- [140] M. Y. Son, Y. J. Hong, J. K. Lee, Y. C. Kang, *Nanoscale* **2013**, *5*, 11592.
- [141] Y. N. Ko, Y. C. Kang, S. B. Park, *Nanoscale* **2013**, *5*, 8899.
- [142] C. M. Sim, Y. J. Hong, Y. C. Kang, *ChemSusChem* **2013**, *6*, 1320.
- [143] S. H. Choi, Y. C. Kang, *ACS Appl. Mater. Interfaces* **2014**, *6*, 2312.
- [144] Y. N. Ko, S. B. Park, Y. C. Kang, *Chem. Asian J.* **2014**, *9*, 1011.
- [145] C. M. Sim, S. H. Choi, Y. C. Kang, *Chem. Commun.* **2013**, *49*, 5978.
- [146] M. H. Kim, Y. J. Hong, Y. C. Kang, *RSC Adv.* **2013**, *3*, 13110.
- [147] S. H. Choi, Y. C. Kang, *ChemSusChem* **2013**, *6*, 2111.
- [148] S. H. Choi, Y. C. Kang, *Chem.–Eur. J.* **2013**, *19*, 17305.
- [149] K. M. Yang, Y. N. Ko, J. Y. Yun, Y. C. Kang, *Chem. Asian J.* **2014**, *9*, 443.
- [150] S. H. Choi, S. K. Park, J. K. Lee, Y. C. Kang, *J. Power Sources* **2015**, *284*, 481.
- [151] S. H. Choi, Y. J. Hong, Y. C. Kang, *Nanoscale* **2013**, *5*, 7867.
- [152] Y. J. Hong, M. Y. Son, B. K. Park, Y. C. Kang, *Small* **2013**, *9*, 2224.
- [153] K. M. Yang, Y. J. Hong, Y. C. Kang, *ChemSusChem* **2013**, *6*, 2299.
- [154] H. J. Kim, H. M. Jeong, T. H. Kim, J. H. Chung, Y. C. Kang, J. H. Lee, *ACS Appl. Mater. Interfaces* **2014**, *6*, 18197.
- [155] S. H. Choi, Y. C. Kang, *Chem.–Eur. J.* **2014**, *20*, 3014.
- [156] S. H. Choi, J. K. Lee, Y. C. Kang, *Nanoscale* **2014**, *6*, 12421.
- [157] Y. J. Hong, J. W. Yoon, J. H. Lee, Y. C. Kang, *Chem.–Eur. J.* **2014**, *20*, 2737.
- [158] S. H. Choi, Y. C. Kang, *Small* **2014**, *10*, 474.
- [159] Y. N. Ko, S. H. Choi, S. B. Park, Y. C. Kang, *Chem. Asian J.* **2014**, *9*, 572.
- [160] Y. N. Ko, Y. C. Kang, S. B. Park, *Nanoscale* **2014**, *6*, 4508.
- [161] S. H. Choi, Y. C. Kang, *ACS Appl. Mater. Interfaces* **2015**, *7*, 24694.
- [162] Z. Y. Wang, D. Y. Luan, C. M. Li, F. B. Su, S. Madhavi, F. Y. C. Boey, X. W. Lou, *J. Am. Chem. Soc.* **2010**, *132*, 16271.
- [163] H. G. Zhang, Q. S. Zhu, Y. Zhang, Y. Wang, L. Zhao, B. Yu, *Adv. Funct. Mater.* **2007**, *17*, 2766.
- [164] J. Liu, H. Xia, D. F. Xue, L. Lu, *J. Am. Chem. Soc.* **2009**, *131*, 12086.
- [165] X. Y. Yu, L. Yu, L. F. Shen, X. H. Song, H. Y. Chen, X. W. Lou, *Adv. Funct. Mater.* **2014**, *24*, 7440.
- [166] J. T. Zhang, H. Hu, Z. Li, X. W. Lou, *Angew. Chem., Int. Ed.* **2016**, *55*, 3982.
- [167] C. C. Yec, H. C. Zeng, *ACS Nano* **2014**, *8*, 6407.
- [168] G. W. Zhan, C. C. Yec, H. C. Zeng, *Chem.–Eur. J.* **2015**, *21*, 1882.
- [169] J. S. Cho, Y. J. Hong, J. H. Lee, Y. C. Kang, *Nanoscale* **2015**, *7*, 8361.
- [170] J. S. Cho, J. M. Won, J. H. Lee, Y. C. Kang, *Nanoscale* **2015**, *7*, 19620.
- [171] J. S. Cho, Y. J. Hong, Y. C. Kang, *ACS Nano* **2015**, *9*, 4026.
- [172] J. S. Cho, Y. C. Kang, *Small* **2015**, *11*, 4673.
- [173] J. S. Cho, S. Y. Lee, H. S. Ju, Y. C. Kang, *ACS Appl. Mater. Interfaces* **2015**, *7*, 25641.
- [174] Y. J. Hong, J. S. Cho, Y. C. Kang, *Chem.–Eur. J.* **2015**, *21*, 18202.
- [175] N. Liu, Z. D. Lu, J. Zhao, M. T. McDowell, H. W. Lee, W. T. Zhao, Y. Cui, *Nat. Nanotechnol.* **2014**, *9*, 187.
- [176] M. Y. Yan, F. C. Wang, C. H. Han, X. Y. Ma, X. Xu, Q. Y. An, L. Xu, C. J. Niu, Y. L. Zhao, X. C. Tian, P. Hu, H. A. Wu, L. Q. Mai, *J. Am. Chem. Soc.* **2013**, *135*, 18176.
- [177] Z. Y. Wang, D. Y. Luan, S. Madhavi, Y. Hu, X. W. Lou, *Energy Environ. Sci.* **2012**, *5*, 5252.
- [178] L. Zhang, R. Rajagopalan, H. P. Guo, X. L. Hu, S. X. Dou, H. K. Liu, *Adv. Funct. Mater.* **2016**, *26*, 440.
- [179] Y. Q. Wang, G. Z. Wang, H. Q. Wang, W. P. Cai, L. D. Zhang, *Chem. Commun.* **2008**, 6555.
- [180] Y. Sheng, H. C. Zeng, *Chem. Mater.* **2015**, *27*, 658.
- [181] F. Zhang, Y. L. An, W. Zhai, X. P. Gao, J. K. Feng, L. J. Ci, S. L. Xiong, *Mater. Res. Bull.* **2015**, *70*, 573.
- [182] X. Wei, C. Tang, X. Wang, L. Zhou, Q. Wei, M. Yan, J. Sheng, P. Hu, B. Wang, L. Mai, *ACS Appl. Mater. Interfaces* **2015**, *7*, 26572.
- [183] F. Z. Mou, J. G. Guan, W. D. Shi, Z. G. Sun, S. H. Wang, *Langmuir* **2010**, *26*, 15580.
- [184] L. M. Lang, D. Wu, Z. Xu, *Chem.–Eur. J.* **2012**, *18*, 10661.
- [185] S. J. Peng, L. L. Li, Y. X. Hu, M. Srinivasan, F. Y. Cheng, J. Chen, S. Ramakrishna, *ACS Nano* **2015**, *9*, 1945.
- [186] J. C. Fu, J. L. Zhang, Y. Peng, C. H. Zhao, Y. M. He, Z. X. Zhang, X. J. Pan, N. J. Mellors, E. Q. Xie, *Nanoscale* **2013**, *5*, 12551.
- [187] Y. J. Hong, J. W. Yoon, J. H. Lee, Y. C. Kang, *Chem.–Eur. J.* **2015**, *21*, 371.
- [188] J. S. Cho, Y. J. Hong, Y. C. Kang, *Chem.–Eur. J.* **2015**, *21*, 11082.
- [189] G. Q. Zhang, B. Y. Xia, C. Xiao, L. Yu, X. Wang, Y. Xie, X. W. Lou, *Angew. Chem., Int. Ed.* **2013**, *52*, 8643.
- [190] X. Wang, M. Y. Liao, Y. T. Zhong, J. Y. Zheng, W. Tian, T. Y. Zhai, C. Y. Zhi, Y. Ma, J. N. A. Yao, Y. Bando, D. Golberg, *Adv. Mater.* **2012**, *24*, 3421.
- [191] X. Wang, Z. H. Chen, D. Q. Liu, W. Tian, Q. Wang, C. Zhang, J. W. Liu, L. Y. Han, Y. Bando, D. Golberg, *Part. Part. Syst. Character.* **2014**, *31*, 757.
- [192] J. M. Tarascon, M. Armand, *Nature* **2001**, *414*, 359.
- [193] M. Armand, J. M. Tarascon, *Nature* **2008**, *451*, 652.
- [194] B. Dunn, H. Kamath, J. M. Tarascon, *Science* **2011**, *334*, 928.
- [195] P. Poizot, S. Laruelle, S. Grugeon, L. Dupont, J. M. Tarascon, *Nature* **2000**, *407*, 496.
- [196] J. Cabana, L. Monconduit, D. Larcher, M. R. Palacin, *Adv. Mater.* **2010**, *22*, E170.
- [197] L. Zhang, H. B. Wu, X. W. Lou, *Adv. Energy Mater.* **2014**, *4*.
- [198] Y. L. Ding, X. B. Zhao, J. Xie, G. S. Cao, T. J. Zhu, H. M. Yu, C. Y. Sun, *J. Mater. Chem.* **2011**, *21*, 9475.
- [199] X. F. Niu, Y. F. Li, Y. J. Hu, H. Jiang, X. Y. Hou, W. G. Li, S. J. Qiu, C. Z. Li, *New J. Chem.* **2016**, *40*, 1839.

- [200] X. L. Ji, K. T. Lee, L. F. Nazar, *Nat. Mater.* **2009**, *8*, 500.
- [201] P. G. Bruce, S. A. Freunberger, L. J. Hardwick, J. M. Tarascon, *Nat. Mater.* **2012**, *11*, 19.
- [202] A. Manthiram, Y. Z. Fu, S. H. Chung, C. X. Zu, Y. S. Su, *Chem. Rev.* **2014**, *114*, 11751.
- [203] S. Q. Chen, X. D. Huang, B. Sun, J. Q. Zhang, H. Liu, G. X. Wang, *J. Mater. Chem. A* **2014**, *2*, 16199.
- [204] P. Simon, Y. Gogotsi, *Nat. Mater.* **2008**, *7*, 845.
- [205] K. R. Yoon, G. Y. Lee, J. W. Jung, N. H. Kim, S. O. Kim, I. D. Kim, *Nano Lett.* **2016**, *16*, 2076.
- [206] M. Gratzel, *Nature* **2001**, *414*, 338.
- [207] J. F. Qian, P. Liu, Y. Xiao, Y. Jiang, Y. L. Cao, X. P. Ai, H. X. Yang, *Adv. Mater.* **2009**, *21*, 3663.
- [208] J. J. Qiu, F. W. Zhuge, X. M. Li, X. D. Gao, X. Y. Gan, L. Li, B. B. Weng, Z. S. Shi, Y. H. Hwang, *J. Mater. Chem.* **2012**, *22*, 3549.
- [209] A. Fujishima, K. Honda, *Nature* **1972**, *238*, 37.
- [210] H. X. Li, Z. F. Bian, J. Zhu, D. Q. Zhang, G. S. Li, Y. N. Huo, H. Li, Y. F. Lu, *J. Am. Chem. Soc.* **2007**, *129*, 8406.
- [211] W. Li, Y. H. Deng, Z. X. Wu, X. F. Qian, J. P. Yang, Y. Wang, D. Gu, F. Zhang, B. Tu, D. Y. Zhao, *J. Am. Chem. Soc.* **2011**, *133*, 15830.
- [212] X. Y. Zeng, J. Yang, L. X. Shi, L. J. Li, M. Z. Gao, *Nanoscale Res. Lett.* **2014**, *9*.
- [213] M. Xu, M. Wang, T. N. Ye, N. Liang, L. Jin, J. T. Zai, X. F. Qian, *Chem.–Eur. J.* **2014**, *20*, 13576.
- [214] B. C. H. Steele, A. Heinzl, *Nature* **2001**, *414*, 345.
- [215] S. J. Guo, Y. X. Fang, S. J. Dong, E. K. Wang, *J. Phys. Chem. C* **2007**, *111*, 17104.
- [216] H. Atae-Esfahani, Y. Nemoto, L. Wang, Y. Yamauchi, *Chem. Commun.* **2011**, *47*, 3885.
- [217] L. Wang, Y. Yamauchi, *J. Am. Chem. Soc.* **2013**, *135*, 16762.
- [218] D. Lee, S. M. Kim, H. Jeong, J. Kim, I. S. Lee, *ACS Nano* **2014**, *8*, 4510.
- [219] G. S. Chai, S. B. Yoon, J. H. Kim, J. S. Yu, *Chem. Commun.* **2004**, *23*, 2766.
- [220] B. Z. Fang, J. H. Kim, C. Lee, J. S. Yu, *J. Phys. Chem. C* **2008**, *112*, 639.